The Cooperative Program for Operational Meteorology, Education and Training (COMET) under Fellowship S04-49759

LOCAL ANTHROPOGENIC AEROSOL SOURCES EFFECT ON WINTER CLOUDS AND PRECIPITATION IN THE COLORADO PARK RANGE

by Daniel S. Ward

William R. Cotton, P.I.

DEPARTMENT OF ATMOSPHERIC SCIENCE

Paper No. 777

LOCAL ANTHROPOGENIC AEROSOL SOURCES EFFECT ON WINTER CLOUDS AND PRECIPITATION IN THE COLORADO PARK RANGE

BY

DANIEL S. WARD

DEPARTMENT OF ATMOSPHERIC SCIENCE

COLORADO STATE UNIVERSITY

FORT COLLINS, CO 80523

RESEARCH SUPPORTED BY

THE COOPERATIVE PROGRAM FOR OPERATIONAL METEORLOGY, EDUCATION AND TRAINING (COMET)

UNDER GRADUATE FELLOWSHIP S04-49759

OCTOBER 6, 2006

ATMOSPHERIC SCIENCE PAPER NO. 777

ABSTRACT.

Recent work has suggested that large amounts of anthropogenic sulfate aerosol reduce riming efficiency in some mixed-phase clouds leading to a decrease in snowfall rate. This study investigates this aerosol effect in the Colorado Park Range for four winter storm cases in February 2005. A dispersion model was employed to simulate particle emission from the Craig and Hayden power plants in northwestern Colorado. The model output was used to determine regions inside the emission plumes (in-plume) and regions outside their influence (ambient air). Then, the cloud environment of the in-plume region was compared to its surroundings using the Moderate Resolution Imaging Spectroradiometer (MODIS) cloud products. Differences in cloud particle size distribution between in-plume and ambient air regions were inconsistent from case to case. The satellite-viewed environment may not have been representative of lower cloud levels due to minimal vertical mixing, typical of orographic storms, and contamination by ice particles as indicated by the MODIS cloud phase product.

To explore possible effects on surface precipitation rate from the power plant emissions, snow-water equivalent (SWE) accumulation data from selected snowpack telemetry (SNOTEL) sites and Storm Peak Laboratory were examined. The average in-plume precipitation rate was less than that of the ambient air for three cases, but the sample size of in-plume sites was small, making analysis difficult. In addition, ranking the snowfall measurements by magnitude demonstrated that there was no observable relationship between precipitation rate and emission plume location in these cases.

Daniel S. Ward
Department of Atmospheric Science
Colorado State University
Fort Collins, CO 80523
Fall, 2006

ACKNOWLEDGEMENTS

I would like to thank Dr. William Cotton for giving me the opportunity to study with him in the Colorado State Atmospheric Science department. I am also grateful to Dr. Chris Kummerow and Dr. Paul Mielke. All the members of the Cotton project group helped this project enormously with instruction and advice. Special thanks to Sue Van Den Heever, Brenda Thompson, Steve Saleeby, Ray McAnelly, Randy Borys, Melanie Wetzel, and Gustavo Carrio for inspiration and for always being happy to help a grad student. This project was supported by a fellowship from the Cooperative Program for Operational Meteorology, Education and Training (COMET) under grant S04-49759. I'd like to give my gratitude to Patrick Dills and Greg Byrd of COMET for their guidance and cheerful assistance.

Many people freely provided me with data for this project. I would like to recognize Chad Campbell (Tri-State Energy), Maggie Dunklee (USDA), Dan Ely (EPA), and Dana Stevens (Xcel Energy) for aiding me in this capacity. Finally, I am greatly indebted to my family for their unending love and support. Thanks especially to Jill for her understanding and motivation during this experience.

TABLE OF CONTENTS

Chapter 1 - Introduction

Recent studies have suggested that anthropogenic aerosols suppress precipitation in mixed-phase clouds by reduced riming of ice crystals (Borys et al., 2000; Borys et al, 2003; Lohmann, 2004). The characteristics and magnitude of this aerosol effect are of considerable interest for climate research (Borys et al., 2000). In addition, as stated by Colle (2004), determining the sensitivity of orographic precipitation to small changes in ambient conditions, such as aerosol concentrations, is a difficult forecast problem. To better understand the impact of aerosols on mixed-phase storms, the current study focuses on the influence of local anthropogenic aerosol sources on cloud microphysics and precipitation in four winter storms in the Colorado Park Range region. This project aims to expand the work done by Borys et al. (2000, 2003) to a regional scale through the use of many surface observations sites and satellite retrievals.

Evidence of anthropogenic aerosol effects on cloud microphysics has been well documented (Leaitch et al., 1992; Lensky and Rosenfeld, 2003; Harshvardhan et al., 2002; Jirak and Cotton, 2006). Increased concentrations of cloud condensation nuclei (CCN) increase the cloud droplet number and thus, for a given liquid water content, decrease the radius of the cloud droplets. This microphysical effect, also known as the second indirect aerosol effect, leads to a suppression of precipitation in polluted clouds (Ramanathan et al., 2001). In mixed-phase clouds, the smaller droplet size can

significantly reduce riming efficiency (Pruppacher and Klett, 1978) leading to a decrease in snowfall rate. In addition, Saleeby and Cotton (2005) found that smaller droplet size leads to enhancement of the Bergeron-Findeisen process which further decreases the liquid water available for riming and reduces the snowfall rate.

The influence of anthropogenic aerosols, as opposed to natural aerosols, is of particular interest in this region because several large anthropogenic sources are located just west of the Park Range. Two studies by Borys et al. (1986, 2000) found that the majority of sulfate measured at a mountaintop site in the Park Range probably originated in coal combustion. Measurements by Pueschel and Van Valin (1978) suggested that the regional CCN budget surrounding coal-fired power generating stations is indeed dominated by the nuclei from this single anthropogenic source. Borys et al. (2003) found that the addition of only a small amount of anthropogenic aerosol reduced the snowfall rate up to 50%. For these reasons, two coal-fired power plants near the Park Range will be the focus of this study.

The impact of these local aerosol sources will be studied using dispersion model output as an estimation of anthropogenic aerosol concentrations. Cloud microphysics and surface precipitation rate for the case studies will then be compared using satellite products and surface precipitation data for estimated clean and polluted regions. Similar methods were used by Harshvardhan et al. (2002) in their study of model output sulfate concentrations effect on marine stratocumulus in the Atlantic. Cloud processes are best studied by in situ investigations, they remark, but these can be prohibitively expensive.

Thus, remote sensing techniques are used. Unfortunately, aerosols cannot be detected remotely in the presence of cloud, motivating the use of model output aerosol estimations in Harshvardhan et al. (2002) and the current study. Wetzel et al. (2004) also noted the need for satellite observations to improve our understanding of snowfall processes in remote mountainous regions. They write that incorporating satellite remote sensing information with observations and model output would greatly improve forecasting techniques specific to orographic scenarios. *In situ* cloud droplet number concentration measurements were available for comparison to satellite retrievals for one of the cases.

Similar results to the in situ observations by Borys et al. (2000, 2003) are expected in the current study. That is, areas with high CCN concentrations (as indicated by model output) will exhibit small droplet sizes and, by reduced riming, a decrease in precipitation rate relative to the region outside the power plant plume influence. It is worth noting that Hindman et al. (1992) did not find a significant relationship between wind direction and cloud droplet number concentrations at a site in the Park Range (as cited by Hindman et al., 1994). However, the high-resolution dispersion model used in the current study will give a better idea where particles may be coming from in the short-range.

The following is a detailed description of the methods and results of this study. In Chapter 2 related studies and current theories of aerosol effects is reviewed to provide background for the interpretation of the results. The sources and collection methods of data used for this study will be described in Chapter 3. This chapter will also include an analysis of the large-scale weather for the four storm cases. In Chapter 4 the model setup

will be explained and the results of the simulations examined. Then, in Chapter 5, the satellite data and surface observations will be analyzed using the model output to infer high aerosol environments. Finally, the conclusions will be outlined and suggestions for future research will be given in Chapter 6.

Chapter 2 - Background

As noted by Seinfeld and Pandis (1998), nucleation of water droplets can occur in the absence or presence of foreign material such as aerosols. Without a foreign substance to act as a nucleus this process is defined as homogeneous nucleation and with, heterogeneous nucleation. However, they explain that only heterogeneous nucleation is realistic in the relative humidity common to the Earth's atmosphere. As such, aerosols are essential to cloud droplet formation and influence precipitation rate. For this reason aerosol effects on cloud microphysics, aerosol chemistry, and aerosol global distribution have been researched extensively. This chapter will review relevant literature on these topics to provide a solid background for the conclusions reached in this Colorado mountain study.

2.1 Aerosols and cloud microphysics

Atmospheric particles that act as droplet nuclei are called cloud condensation nuclei (CCN). Not all aerosols are considered CCN since the ability to nucleate a droplet depends on the aerosols' qualities, mainly size and solubility. Several studies have shown that aerosols composed of a large water-soluble fraction are more likely to act as CCN (Leaitch et al., 1992; Boucher and Lohmann, 1995; Hallberg et al., 1994). The relationship between aerosol size distribution and CCN number is also well documented,

and it is generally agreed that large aerosol are more likely to serve as CCN (Novakov et al., 1994; Leaitch and Isaac, 1994). Aerosol size and composition varies greatly and will be discussed in more detail later in this chapter.

Since atmospheric water droplets will only form in the presence of CCN, the cloud droplet number concentration (CDNC) of a cloud is strongly related to the local CCN concentration. An environment with high CCN concentrations will likely develop a cloud with a high CDNC. This relationship was demonstrated experimentally in 1960 by Squires and Twomey (as cited by Twomey, 1974) and validated in a study by Twomey and Warner from Queensland, Australia (1967). Using measurements of CDNC and CCN in small to moderate sized non-precipitating cumuli Twomey and Warner (1967) found strong agreement between the CDNC observed in-cloud and the expected CDNC calculated from the nuclei measurements. It should be noted that the suggested relationship between CCN concentration and CDNC is not one-to-one. According to Twomey and Warner's (1967) results, the ratio of CCN:CDNC depends on the ambient supersaturation which, in turn, is related to the environment's updraft speed. Subsequent work by Leaitch et al. (1992) showed a correlation between CDNC and sulfate aerosol using data from approximately 400 cloud water samples of continental stratiform and cumuliform clouds. In contrast, a study by Novakov et al. (1994) found no statistical dependence of sulfate aerosol on CDNC in cumulus clouds and only weak dependence in stratocumulus clouds. However, the more recent Novakov et al. (1994) measurements were taken at a marine location. Also, measurements of non-sulfate aerosol during this

study suggest that sulfate may not be a major influence on cloud microphysics in this environment.

In addition to influencing droplet number, aerosol acting as CCN also affect the droplet size distribution. Consider two clouds containing an equal amount of liquid water but drastically different CCN concentrations. The high-CCN cloud will hold more droplets relative to the low-CCN cloud and therefore, since the water amount is limited, produce smaller droplets. This decrease in droplet radius with an increase in CCN number was recognized by Gunn and Phillips (1957) and has been the focus of many investigations into aerosol effects on cloud radiative properties. Twomey (1977) provides a summary of this process. He explains how an increase in aerosol concentration may increase the CDNC, thereby decreasing droplet size and leading to an enhanced cloud albedo. This effect is known as the "Twomey effect" and has been demonstrated in satellite observations by Rosenfeld (1999).

In fact, several recent studies have shown evidence of aerosol effects on CDNC and droplet radius by utilizing satellite retrievals (Lensky and Rosenfeld, 2003; Rosenfeld, 1999; Breon et al., 2002). Research satellites have large, often global, areal coverage and typically take daily observations. These characteristics make satellite retrievals convenient for studying regional and global cloud properties. There do exist limitations in the quality of satellite estimations that make *in situ* measurements essential for any *quantitative* study of aerosol effects on global cloud microphysics (Breon et al., 2002). Still, satellite retrievals provide evidence of aerosol-cloud effects in different weather

regimes all over the globe. Reflectance measurements from the Advanced Very High Resolution Radiometer (AVHRR) were used by Harshvardan et al. (2002) to suggest that anthropogenic sulfate reduced droplet size in maritime clouds over the Atlantic Ocean. Rosenfeld (2000) presented striking images of power plant pollution plumes visible in satellite retrievals of droplet radius also derived from AVHRR reflectance measurements. The small droplet radius tracks shown in Rosenfeld (2000) were identified in clouds with tops above -12˚C, or warmer than many northwestern Colorado winter clouds. These satellite studies have made plain the feasibility of using satellite retrievals to demonstrate aerosol effects on clouds, if only indirectly.

2.2 Aerosol effects on precipitation

While much attention has been given to the effects of aerosols on cloud radiative properties, changes in CDNC and droplet radius resulting from variations in aerosol concentration affect the precipitation process as well. Nearly 50 years ago, Gunn and Phillips (1957) found that clouds forming in clean (nearly particle-free) air developed precipitation faster than polluted (particle-rich) air. Their experiments, which were done in a large spherical cloud chamber, suggested a relationship between aerosol concentration and precipitation efficiency that has been validated many times since.

An increase in CCN concentrations prevents large droplet formation, leading to a narrowing of a cloud's droplet size distribution. In warm clouds (clouds consisting of only liquid water) this narrowing of the droplet size distribution causes a decrease in the

droplet collection efficiency and inhibits large droplet growth (Lensky and Rosenfeld, 2003).

For cold, mixed-phase clouds common to the Colorado Park Range in winter, precipitation depends largely on the riming of snow ice crystals. Larger droplets rime more efficiently than smaller droplets, suggesting that aerosols could significantly affect precipitation in mixed-phase clouds (Borys et al., 2000). In fact, droplets with diameters less than 10 microns (referred to as the "critical riming size" by Borys et al. (2000)) are not collected by snow crystals of any size (Pruppacher and Klett, 1978). An *in situ* study by Borys et al. (2003) at Storm Peak Lab in Steamboat Springs, Colorado showed a reduced precipitation rate during a high aerosol concentration event when compared to a cleaner storm. The average droplet radius during the high aerosol concentration event was below the critical riming radius.

Saleeby and Cotton (2005) tested the sensitivity of model simulations of winter orographic clouds to changing CCN and giant CCN (GCCN) concentrations. They found reduced riming rates for simulations with a high initial CCN concentration because, similar to Borys et al.'s (2003) conclusions, riming efficiency was reduced as droplet size decreased. They also showed that, since smaller droplets evaporate more quickly than larger droplets, less liquid water was available for riming in the high CCN simulations leading to even less surface precipitation. The addition of GCCN into the cloud simulations increased surface precipitation in high CCN environments by creating large droplets that collide and coalesce efficiently. In contrast, GCCN reduced surface

precipitation for low CCN environments because of the increased competition for vapor deposition between droplets. The presence of GCCN may be important for this study because coal power plant emissions have been shown to include higher GCCN concentrations than the ambient air (Mamane and Pueschel, 1980).

2.3 Anthropogenic aerosol species

As aforementioned, not all aerosols act as CCN. The varying chemistry of different aerosol species has implications for the magnitude of their effect on clouds and precipitation. Aerosol species can be divided into natural and anthropogenic categories. Natural species such as sea-salt and mineral-dust do affect cloud microphysics in the Park Range. However, in continental locations, the anthropogenic contribution to aerosol concentrations typically overshadows the natural contribution (Hudson, 1991). As anthropogenic aerosol likely have a significant impact on the weather in the Park Range, they will be discussed here.

The two most abundant anthropogenic aerosol species affecting CCN are known as sulfates and nitrates (Leaitch et al., 1992). Both of these are secondary aerosol, meaning they are not emitted from the surface but formed through chemical reactions in the atmosphere. Sulfates and nitrates contribute to atmospheric CCN either by forming particles through chemical reactions or by depositing on an existing particle and increasing its solubility.

2.3.1 Nitrates

The nitrates include all atmospheric particles that contain NO_3^- in some capacity. The most common soluble nitrate species in the atmosphere are particulate nitrate (p - NO_3^-) and nitric acid (HNO_3). These two species are also the greatest contributors of nitrate in cloud water, suggesting they make the most CCN of all the nitrates (Leaitch et al., 1992). The creation of both particulate nitrate and nitric acid relies on reactions involving NO or NO_2, two gases which together are referred to as NO_X – a primary product of coal-fired power plants. Particulate nitrate results from interactions between gaseous nitrogen species and atmospheric particles. This often occurs between gaseous nitric acid and soil and sea-salt particles (Pakkanen, 1996). Nitric acid aerosol are formed by the following reactions, as shown in Seinfeld and Pandis (1998):

During the day,

$OH^- + NO_2 > HNO_3$

And at night,

$O_3 + NO_2 > NO_3^- + O_2$

$NO_2 + NO_3^- <> N_2O_5$

$N_2O_5 + H_2O > 2\ HNO_3$

The nitric acid that is produced by these reactions often reacts with atmospheric ammonia (NH_3) to form ammonium nitrate (NH_4NO_3). Ammonium nitrate is a locally important

aerosol species in terms of direct radiative forcing according to Haywood and Boucher (2000) and as an efficient CCN (Metzger et al., 2002), but only forms in low-sulfate environments (Seinfeld and Pandis, 1998). In a high-sulfate environment, such as in a coal power plant plume, the contribution of NO_X emissions to local ammonium nitrate concentrations and thus local CCN will be severely limited.

2.3.2 Sulfates

Sulfate aerosol has received a lot of attention in atmospheric research due to its global abundance and far reaching effects on weather and climate. Ten studies of atmospheric sulfur emissions reviewed by Haywood and Boucher (2000) estimate the global atmospheric sulfate burden to be between 1.5 and about 3 Tg SO_4. In the majority of cases the anthropogenic contribution to the global sulfate burden was greater than the natural contribution. As well as being plentiful, atmospheric sulfate is a major component of the *soluble* continental aerosol (Borys et al., 2000). Because of its abundance and solubility, sulfate aerosol is often used as a surrogate for CCN in studies of continental aerosol effects on clouds and precipitation (Leaitch and Isaac, 1994; Novakov et al., 1993; Borys et al., 2000; Boucher and Lohmann, (1995)).

The main source of anthropogenic sulfate aerosol is via sulfur dioxide (SO_2) emissions from fossil fuel burning (Haywood and Boucher, 2000). 56% of the world's sulfur emissions in 1990 were from coal (Smith et al., 2001). According to Boucher and Lohmann (1995), SO_2 forms sulfate aerosol, typically in the form of sulfuric acid

(H_2SO_4), through two main processes. They describe how SO_2 can be oxidized into sulfuric acid in the gas-phase by the hydroxyl radical (OH), then either condense onto existing particles or form a new particle by homogeneous nucleation. In addition, they explain that a large fraction of SO_2 is oxidized in the liquid phase of cloud droplets. The liquid-phase oxidation occurs on a shorter time-scale than the gas-phase oxidation and is potentially a greater source of sulfate for short-range chemical transports. This process is dependent on the amount of available dihydrogen dioxide (H2O2) in the atmosphere, a substance that is often limited in the winter (Kleinman and Daum, 1991).

2.4 Coal-fired power plant plume attributes

Coal-fired power plants are large sources of sulfur dioxide and NO_X, and thus large sources of CCN. Mamane and Pueschel (1980) give a quantitative example of just how large these sources can be in their analysis of the Four Corners Power Plant plume. This coal-fired power plant emits 13,428 kg of sulfur dioxide into the atmosphere every hour, or close to 130,000 tons per year. The Craig and Hayden power plants are comparably cleaner, keeping in mind the Four Corners measurements were taken in 1978 before contemporary pollution controls were put into place. The Hayden and Craig coal-firing units combined emit approximately 13,000 tons of SO_2 and 26,000 tons of NO_X every year (Mast et al., 2005).

The rate of aerosol, specifically sulfate, production in power plant plumes has been measured from the air in several studies with varying results (Hobbs et al., 1980; Cantrell

and Whitby, 1978; Husar et al., (1978)). The observations agree that the rate of sulfate production is significantly higher during the day than at night. Pueschel and Van Valin (1978) note that the in-plume sulfur dioxide oxidation rate depends on the local humidity. They found the highest rate of sulfate production occurred when the relative humidity exceeded 50%, lending support to an accelerated liquid phase oxidation of SO_2. The majority of observations in these studies put the SO_2 oxidation rate between 0.5% and 2% SO_2 per hour during the day and below 0.5% SO_2 at night.

To understand the impact of a power plant on the local or regional climate, as stated by Mamane and Pueschel (1980), it is necessary to estimate the production rates of CCN. According to their *in situ* measurements, CCN forms at an estimated rate of 10^{16} - 10^{17} s^{-1} in the Four Corners plume. Similar rate estimates were found by Pueschel and Van Valin (1978) and Hobbs et al. (1980). Also, Mamane and Pueschel's (1980) measurements showed that the in-plume concentration of large particles with diameters from 1-10 microns was significantly higher than the concentration in the ambient air, establishing that coal power plants add significant quantities of GCCN as well as CCN to the atmosphere. Of course, the incredibly high levels of CCN produced will diffuse rapidly as the plume advects away from the source. Still, in a study of the same Four Corners power plant, Pueschel and Van Valin (1978) stated that CCN within the plume steadily increases with horizontal distance from the source sulfur dioxide has more time to oxidize.

Measurements of cloud droplet number concentration by Hobbs et al. (1980) found that droplet number inside the power plant plume were about an order of magnitude greater than that measured in the ambient air for stratiform clouds. In cumulus clouds the effect of the plume emissions on cloud droplet number concentration could not be distinguished from natural variability (Hobbs et al., 1980).

The literature reviewed suggests a reduction in surface precipitation should be expected in locations under the influence of the Craig and Hayden power plant emission plumes. High CCN concentrations within the power plant plumes should cause an increase in droplet number and a decrease in droplet size. The smaller droplets within the plume will not rime efficiently and precipitation will be reduced. Next the data and methods used for testing this theory for Park Range snowstorms will be discussed.

Chapter 3 - Data Sources

Many strategies have been employed to investigate the second indirect aerosol effect, as shown in the previous chapter. These have included remote sensing, aircraft, modeling, and mountain laboratory research. For this research a combination of data sources has been employed including model output (see Chapter 4), satellite retrievals, and mountain surface observations. Chapter 3 will introduce the study region and winter storm cases, as well as describe the collection, quality and intended use of the satellite and ground-based data.

3.1 Study region

The region of focus lies roughly within the lines of longitude 109˚W - 105˚W and latitude 39˚N - 42˚N. Essentially, this includes the northwestern corner of the state of Colorado and a small portion of south-central Wyoming. The local topography is shown in Figure 3.1. It is characterized by the mountains of the Park Range to the east rising out of a comparably level area to the west. Outside of the study area the higher peaks of the Colorado Rockies lie to the south and east. The Wasatch Range in Utah is located to the west at about 111˚W - 110˚W longitude. To the southwest the terrain is relatively flat and rises steadily to the east toward the Colorado Rockies. These large topographic

features will affect the studied weather systems on a large scale, but the time and spatial scales being investigated are small enough that the effects of the local topography will likely overshadow the large-scale influences. The locations of the Craig and Hayden power stations are marked in Figure 3.1. They lie in the Yampa Valley, a largely agricultural landscape surrounded on three sides by high spruce forest covered terrain. The Storm Peak Laboratory (SPL) is located due east of the power plants and in the Park Range high country at an elevation of 3210m (Borys and Wetzel, 1997) and is also marked in Figure 3.1.

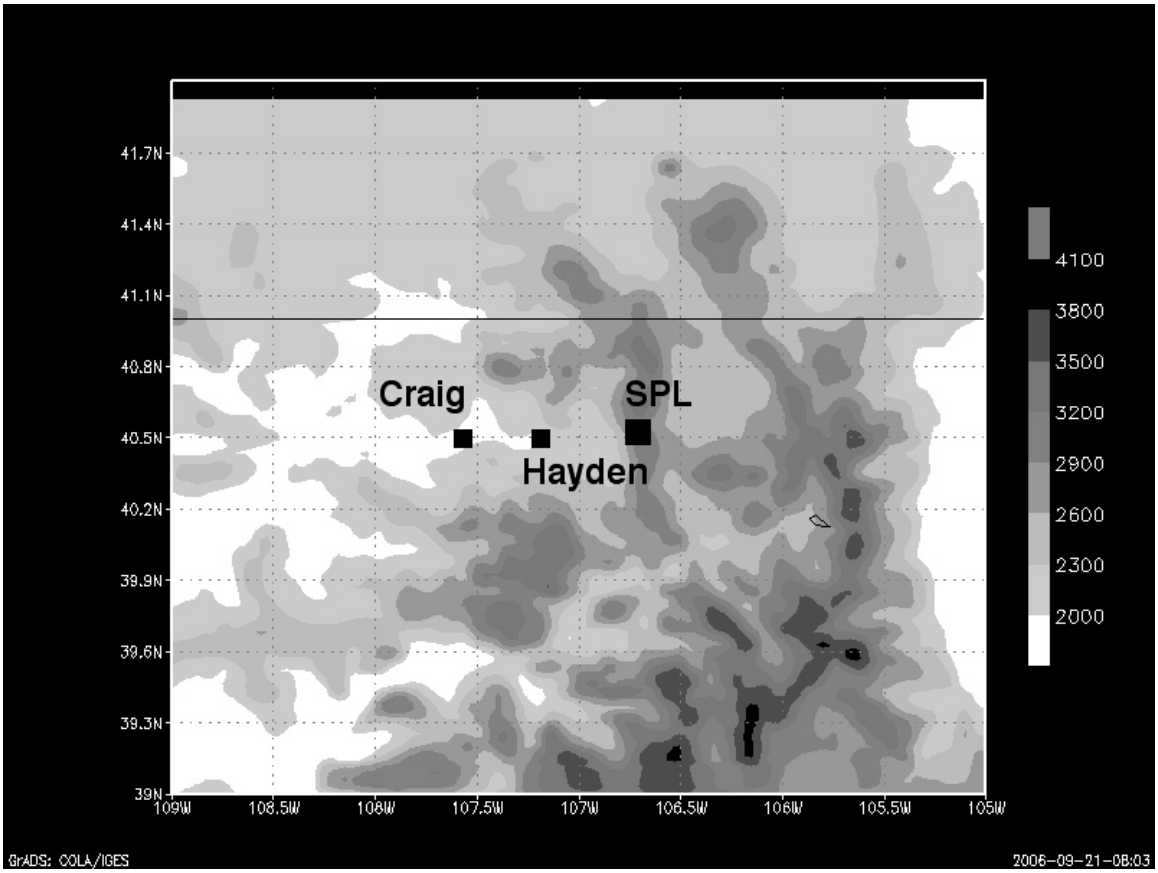

Figure 3.1: Elevation (in meters) of the northwestern Colorado study region. The locations of the Craig and Hayden power plants and SPL are marked for reference.

3.1.1 Park Range topography

The Park Range area was chosen for several reasons. First, owing to its topography, the Park Range is an ideal location for studying orographic winter storms. Orographic clouds are defined by Rauber et al. (1986) as clouds that form in response to a strong cross-barrier pressure gradient but are not directly associated with a large-scale cyclonic disturbance. These clouds can form precipitation or enhance precipitation when embedded in a large-scale system. The formation and enhancement of precipitation can be caused by several mechanisms but all typically result in an increase in precipitation on the barrier windward slope and crest (Colle, 2004), a supposition confirmed for the Park Range by Borys et al.'s (2000) measurements.

As noted by Rauber et al. (1986) the Park Range runs perpendicular to the predominantly westerly flow that occurs during many storm periods. This, along with the large elevation difference between the Yampa Valley floor and the Park Range barrier, create a model setup for orographic clouds and precipitation enhancement. With the Flat Tops mountain region located to the south and west of the Park Range, a large-scale northwest flow is ideal for orographic lift in northwestern Colorado. Not surprisingly, Hindman et al. (1994) reports that SPL is often shrouded in cloud during the winter months, providing ample opportunity for study of orographically influenced storms. The frequency of these storms means that anthropogenic influences on the storm microphysics could have a large impact on the local climate.

3.1.2 CCN concentrations and observations in the Park Range

Another advantage the Park Range atmosphere holds for this study is its generally low CCN concentrations. In such a pristine environment the impact of isolated anthropogenic aerosol sources is substantial. Several studies have provided evidence of the low climatological CCN levels in northwestern Colorado (Borys et al., 2000; Hindman et al., 1994; Rauber and Grant, 1986). Rauber and Grant (1986) list several reasons for the low CCN concentrations they found from aircraft observations over the Park Range. They write that winter snow-cover inhibits mechanical interaction between the atmosphere and the surface, diminishing the importance of this natural aerosol source. Furthermore, they contend that distant mountain ranges, such as the Wasatch and Uinta ranges in Utah, scavenge CCN before it reaches Colorado. Perhaps most importantly, they state that northwestern Colorado is practically void of large anthropogenic sources of CCN, though notably they mention the exception of isolated power plants.

Two of the "exceptions" are the Craig and Hayden coal-firing power plants. Recall that past work has shown that isolated anthropogenic aerosol sources can drastically affect cloud microphysics in a low aerosol background environment. Craig and Hayden's proximity to the Park Range (within 60 km west of SPL) make them worthy of note in this region. Add to the location the large amounts of SO_2 and NO_X being emitted, and its constancy, and the Craig and Hayden plants are very likely the two most important anthropogenic aerosol sources in the vicinity.

Of course, even in this remote region they are not the only source of anthropogenic aerosol. The towns of Craig and Hayden themselves, as well as the city of Steamboat Springs, are small urban centers within the study area that undoubtedly contribute CCN to the environment. Their contribution may be limited by inversions that frequently form above the boundary layer during the winter in the northern Colorado Rockies (Rauber and Grant, 1986). The inversions limit mixing between boundary layer air and the midlevel cloud layers over broad areas according to Rauber and Grant (1986), a limitation that power plant emissions may be able to break through due to the height at which emissions occur and the initial buoyancy of the plume. These characteristics of power plant plumes will be discussed in detail in Chapter 4.

Other possible CCN sources near the Park Range include the more substantial city of Grand Junction, Colorado, and other industrial plants near Rock Springs and Rawlins, Wyoming and Vernal, Utah. Grand Junction lies just outside the study area, approximately 200km southwest of Craig, Colorado. The Jim Bridger plant near Rock Springs is located about 150km to the north of the Park Range and emits on average about 20,000 tons of SO_2 annually (compare to Craig/Hayden's 13,000 tons of SO_2). About 100 miles east of the Jim Bridger plant lies the Sinclair oil refinery, near Rawlins, Wyoming. These two aerosol sources could potentially contribute large amounts of CCN to the Park Range region for a north to northeasterly large-scale wind. As noted by Rauber and Grant (1986) and Borys and Wetzel (1997), the prevailing wind flow across the Park Range is westerly, suggesting that the Wyoming sources may not have a large

climatological impact on the Park Range. Their possible influences for the cases examined in this study will be considered.

The Bonanza plant outside of Vernal Utah is just outside the study area and located west of the Craig and Hayden plants but produces only about one tenth of the SO_2 emitted at Craig and Hayden. In all probability these additional CCN sources are minor CCN suppliers to the Park Range compared to the Craig and Hayden plants and are generally not included in this study. However, since aerosol concentrations are not directly measured for the case studies, the possible impact of these and other CCN sources must be considered in this study's conclusions.

Finally, the SPL and the numerous snowpack telemetry (SNOTEL) observation sites within the study region make it an excellent setting for this study. SPL provides in-cloud measurements of cloud microphysics and now CCN, and the SNOTEL observation system collects hourly snowfall totals over the entire Park Range area.

3.2 Case studies

The Park Range region provides ample winter storm events for scrutiny. Several criteria were used to find appropriate case studies for this research. First, data availability limited the choice of case studies to the winters of 2002-2005. Secondly, it was required that the storm events produce measurable precipitation over a majority of the study region around the same time as a Moderate Resolution Imaging Spectroradiometer (MODIS) instrument

passed over (the *Terra* satellite usually passes around 18:00Z). Otherwise a regional assessment of cloudtop droplet characteristics would be unavailable. Finally, the storm cloud must contain some liquid water at cloud top as indicated by MODIS products. Rauber et al. (1986) found liquid water in all stages of orographic storms in the Park Range and Rauber and Grant (1986) reported supercooled liquid droplets at cloud tops for most of these storms although this is not always the case. A storm that took place on February 7 was considered for this study but later dropped because the MODIS cloud phase product indicated the storm clouds were entirely glaciated. Very little information about the liquid water microphysics could be discerned.

Four storms were chosen for this study occurring mainly on February 12, 15, 19, and 22 of 2005. These storms are unremarkable aside from fitting the criteria laid out above. Conveniently, during these storms all five coal-firing units at Craig and Hayden, which are periodically shut down for maintenance, were in operation ensuring maximum aerosol production. Even though this study focuses on small-scale meteorology, knowledge of the large-scale character of these winter storms may provide insight into differences between each case. The following are brief synoptic overviews of the four case studies. All synoptic maps were generated using the National Centers for Environmental Prediction's (NCEP) North American Regional Reanalysis (NARR) dataset. This dataset was also used for model initialization in this project and will be discussed in detail in Chapter 4.

3.2.1 February 12 case

Snow fell across most of western Colorado on February 12, 2005 though it was, for the most part, a light snow event. Figure 3.2 shows the 500mb geopotential heights and geostrophic absolute vorticity for 18Z on the 12th. This roughly corresponds to the timing of the MODIS instrument overpass and will be the time of greatest scrutiny of the storm.

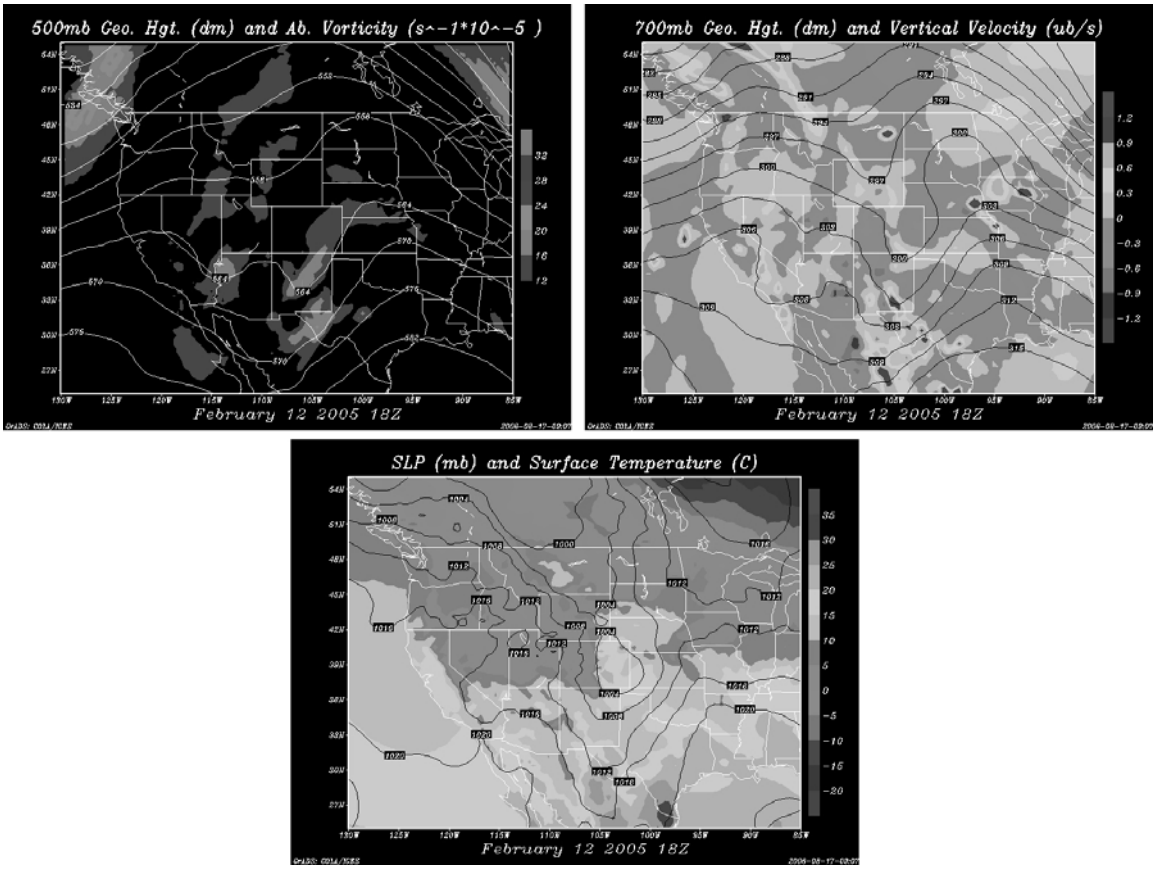

Figure 3.2: Synoptic weather maps for 18:00Z February 12, 2005. 500mb geopotential heights (contours - dm) and absolute vorticity (shaded - s^(-10^-5)) top left; 700mb geopotential height (contours - dm) and vertical velocity (shaded - ub/s) top right; Surface sea level pressure (contours - mb) and surface temperature (shaded – ˚F) bottom.

At this time a short wavelength 500mb trough is located over the Central Rockies. This trough will intensify and move east over night but at 18Z its presence was felt in northwestern Colorado as it brought westerly winds over the peaks of the Park Range.

A west wind, favorable for some orographic lifting in the study region, can be discerned in the this case at the 500mb and 700mb (see Figure 3.2) pressure levels by assuming geostrophic flow at both. This assumption may break down at the 700mb level over the Park Range as the land surface is high enough to induce frictional slowing of the 700mb wind. The geopotential heights at the 700mb level still provide an accurate approximation of wind speed and direction if approaching the Park Range from lower elevations to the west and north. Also visible on the 700mb map is an area of rising air along the western slopes of the Colorado Rockies. This may be evidence of orographic lifting and certainly suitable conditions for a precipitation in this area.

The surface map (see Figure 3.2) shows a low pressure center forming at the surface east of the Rockies and an incursion of warmer air. A corresponding influx of cold air on the western slopes has brought surface temperatures below freezing in the study area. Similarly drastic advection of cold air was seen in mid-levels of the atmosphere leading to a probable shut-down of synoptic scale lift. Therefore this event was in all likelihood mainly orographic in nature with large-scale subsidence surrounding a small area of strong lift upwind of the mountains.

3.2.2 February 15 case

February 15th saw moderate snowfall with well over 1 cm of accumulated snow-water equivalent (SWE) reported at some mountain sites, mostly contained within northwestern Colorado. The upper atmosphere appeared very different on this occasion than on February 12th. Figure 3.3 shows zonal flow at 500mb across the central United States with an area of mainly shear-generated vorticity to the north and west of the Park Range.

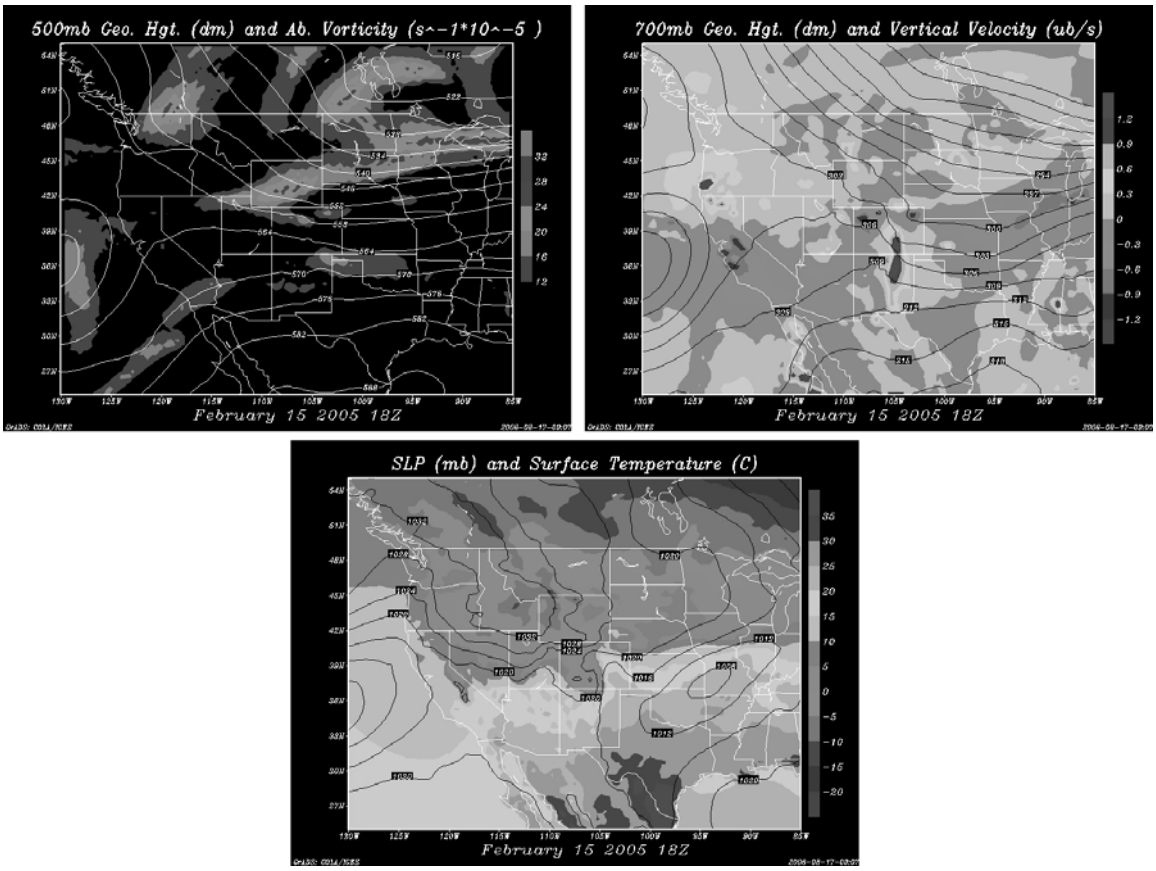

Figure 3.3: Synoptic weather maps for 18:00Z February 15, 2005. 500mb geopotential heights (contours - dm) and absolute vorticity (shaded - s^(-10^-5)) top left; 700mb geopotential height (contours - dm) and vertical velocity (shaded - ub/s) top right; Surface sea level pressure (contours - mb) and surface temperature (shaded – ˚F) bottom.

As on the 12th, wind at 500mb and 700mb (see Figure 3.3) were generally westerly over the study region though more intense at 500mb in this case.

A small area of intense rising air is evident at 700mb practically centered on Craig, Colorado. This lines up well with the location of the resultant snowfall. The surface map (see Figure 3.3) is dominated by a high pressure center to the northwest and a north-south pressure gradient over the study area suggesting generally west winds at the surface. Temperature advection at the surface and aloft was rather innocuous in this case. Again, it appears the February 15th precipitation was largely due to orographic lifting. In contrast to the lighter snowfall on the 12th, this case may have been enhanced by vorticity advection at 500mb, more intense upper level westerly wind, and a lack of the large-scale subsidence seen on the 12th.

3.2.3 February 19 case

The February 19th snow was a mountain event. Low elevations, such as the Yampa Valley, saw low precipitation totals and also saw mostly rain. The setup for this event is apparent in the lines of geopotential height at 500mb and 700mb shown in Figure 3.4. The flow at these levels brought moist and relatively warm air up from the southwest, originating over the Pacific Ocean. Small disturbances in the 500mb course are evident as areas of high absolute vorticity and may have provided pulses of rising and sinking air throughout the day.

Yet again the wind at 500mb and 700mb is upslope in northwestern Colorado, though not oriented nearly orthogonal to the Park Range as in the previous two cases. The vertical velocity at 700mb shows the area of greatest lift in Colorado in the southwestern corner, upwind of the San Juan Mountains. Due to the orientation of the flow, the San Juans are positioned to benefit most from orographic lift in this case.

At the surface, central Colorado sat under a low pressure center which intensified and moved east with time, as is the typical pattern on the leeward side of the Rockies (see

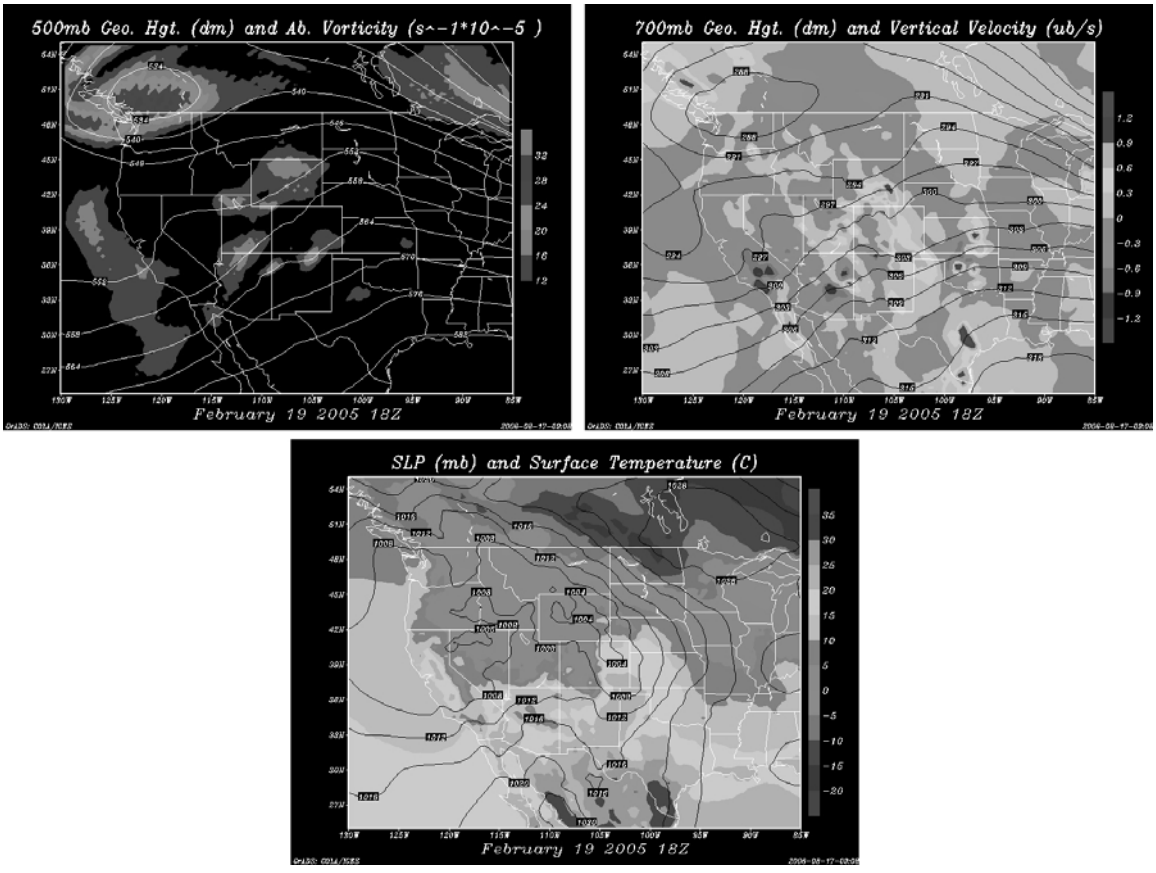

Figure 3.4: Synoptic weather maps for 18:00Z February 19, 2005. 500mb geopotential heights (contours - dm) and absolute vorticity (shaded - s^(-10^-5)) top left; 700mb geopotential height (contours - dm) and vertical velocity (shaded - ub/s) top right; Surface sea level pressure (contours - mb) and surface temperature (shaded – ˚F) bottom.

Figure 3.4). On the 19th this developing storm was still young and had little effect on the flat pressure gradient that existed over the study area. The temperature contours show that western Colorado was indeed warmer than freezing at the surface. Clearly the orographic lift and synoptic-scale lift in the Park Range were minimal on the 19th. This storm did have the advantage of ample moisture supply that was enough to produce moderate snowfall in the mountains, especially in those areas that are unobstructed to the southwest.

3.2.4 February 22 case

Light snow amounts fell in the mountains on February 22nd and light rain in the low elevations to the west. The storm responsible for this precipitation was remarkably different that the previous three cases. In the mid to upper levels of the atmosphere this storm was characterized by weak flow (see Figure 3.5). Geostrophic heights at 500mb and 700mb indicate very weak westerly wind was possible over the study region, but not likely. The main atmospheric feature in the western U.S. at this time was an intense upper-level low off the coast of southern California and cut-off from the main flow through 300mb. At 500mb a deformation zone, where high amounts of upper level divergence can occur, is positioned just west of the study region at 18Z. In fact the Utah highlands did see large snow totals from this storm, though the 700mb vertical velocity contours suggest strong subsidence in southern Utah.

The deformation zone may not have been near enough to northwestern Colorado to have an impact but the 700mb map indicates large-scale rising motion over much of Colorado. The surface map (Figure 3.5) hints at possible northerly winds near the surface in eastern and central Colorado but shows the study area in a region of little pressure change. In summary, on the 22nd a large area of rising air was located over Colorado and included the Park Range. The cause of the lift is not obvious, though orographic forcing may have played some part.

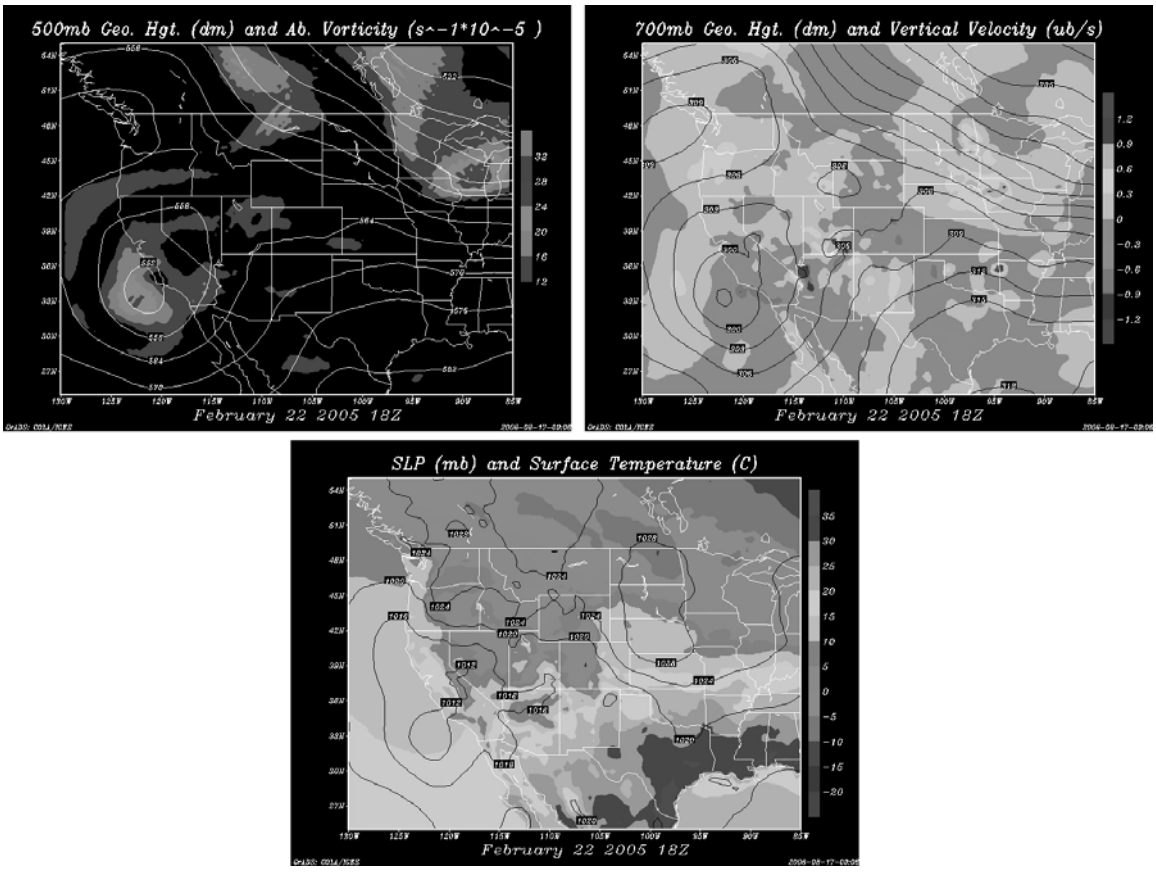

Figure 3.5: Synoptic weather maps for 18:00Z February 22, 2005. 500mb geopotential heights (contours - dm) and absolute vorticity (shaded - s^(-10^-5)) top left; 700mb geopotential height (contours - dm) and vertical velocity (shaded - ub/s) top right; Surface sea level pressure (contours - mb) and surface temperature (shaded – ˚F) bottom.

All four of the case study storms produced precipitation across most of the study region, but all were results of very difference synoptic situations. While this is a great example of how large an impact orographic lifting can have on local weather, the variations in storm dynamics need to be taken into account when forming conclusions about the effects of aerosols.

3.3 MODIS products

Many studies have shown the usefulness of solar reflectance measurements in the visible and near-infrared wavelengths from satellites for estimating cloud parameters remotely (Kaufman et al., 1990; Platnick et al., 2001; Wetzel et al., 2004; Nakajima et al., 2001). The MODIS instrument measures solar reflectance and brightness temperature in these wavelengths and with horizontal resolution as fine as a few hundred meters for some channels. MODIS takes these measurements from approximately 705km above the Earth's surface aboard the National Aeronautics and Space Administration (NASA) Earth Observing System (EOS) *Terra* and *Aqua* satellites (Platnick et al., 2003). Both satellites are polar-orbiters, circling the Earth in a sun-synchronous orbit. They each scan a swath of 2330km, large enough to cover the globe every two days (Platnick et al., 2003).

Specifically, MODIS observes the solar reflectance and brightness temperature of the Earth and atmosphere in 36 spectral bands between wavelengths of 0.4 and 14.5 microns (Li et al., 2003). Since cloud properties affect the amount of radiation reflected back to

the satellite, and the amount of reflection can also vary with wavelength, many cloud parameters can be estimated from space. Algorithms have been developed to estimate cloud properties such as liquid water content, particle phase and particle size, from MODIS reflectance measurements. Data products created by the algorithms have countless applications in global atmospheric research. Here they will be used to observe regional effects of power plant emissions on cloud microphysics. There are, of course, limitations to the accuracy of the MODIS product algorithms' estimations of cloud properties. The following sections will discuss the development and shortcomings of MODIS products that are relevant to this study.

3.3.1 Cloud mask

To determine cloud properties from a MODIS retrieved data pixel, first it must be established whether or not a cloud exists in that area. The MODIS cloud mask product is the end result of a series of tests used to assess the likelihood of a pixel being obstructed by clouds (Platnick et al., 2003).

The tests used to produce the cloud mask product were developed by Ackerman et al. (1998). They write that clouds generally exhibit higher reflectance and lower temperature than the Earth's surface but many factors can dim the contrast between cloud and surface from a satellite's standpoint. For example, bright clouds may be difficult to distinguish from the Earth's surface if they are being viewed over snow and ice. Snow

and ice can be both bright and highly variable in the visible wavelengths, both acting to increase uncertainty in retrieving cloud parameters (Platnick et al., 2001).

The cloud mask algorithms described by Ackerman et al. (1998) utilize 14 of the 36 MODIS-observed spectral bands to mitigate these problems, though the more recent Platnick et al. (2003) work mentions that up to 20 channels may be used. The tests consist of brightness temperature difference checks, reflectance threshold tests and reflectance ratio tests, all of which give a "yes" or "no" answer (Ackerman et al., 1998). The end result is 48 bits of information per pixel that includes information about individual test results, the land surface and the type of clouds that may exist (Platnick et al., 2003). The first two bits classify the pixel in question as one of four descriptors: "confident clear", "probably clear", "uncertain/probably clear", or "cloudy".

These designations are based on the level of confidence that the pixel is *clear*. This is an important distinction, according to Platnick et al. (2003), because it means a "cloudy" pixel is not necessarily overcast and may not be suitable for a retrieval of optical thickness and particle size. Typically, this winter storm study will deal with truly overcast pixels. But it remains important to consider that erroneous values may still exist due to non-overcast "cloudy" pixels. Especially in light of the fact that a greater number of cloud mask errors occur over high elevation regions (Platnick et al., 2003).

3.3.2 Cloud thermodynamic phase

For this project only liquid water pixels are useful for analysis. Anthropogenic sulfate and nitrate are not expected to have a large affect on ice particle concentrations. Therefore the pixels containing liquid water are separated from those containing ice by the cloud thermodynamic phase product.

Differences in the radiation absorption characteristics of water and ice particles at various wavelengths make distinguishing water from ice in clouds possible. King et al. (1997) explains that reflectance in the visible wavelengths is barely affected by particle thermodynamic phase. They go on to describe how at longer wavelengths, such as MODIS channels at 1.64 and 2.13 microns, the reflectance of an ice cloud will be smaller than that of a liquid water cloud. Particle phase is assessed by comparing the reflectance at the reference visible wavelength (0.645 microns in this case) to that at the 1.64 or 2.13 micron wavelength. Since King et al. published their MODIS algorithms, a new method for determining phase has been put into place. The brightness temperature difference between the 8.5 and 11 micron bands is used to retrieve cloud phase. This method has the advantage of being available for both day and night retrievals since it is not based on solar reflectance measurements.

Of course, the process of determining cloud phase is not that simple. Often ice crystals and water droplets are mixed together. These mixed-phase clouds are most prevalent when cloud top temperature ranges from 233-273K (Platnick et al., 2003). The cloud

tops studied in northwestern Colorado have temperatures in this range and Rauber et al. (1986) indicated that mixed-phase cloud tops are common during winter in this region. Therefore it is impossible to avoid ice contamination in other cloud-top products, such as particle radius, for the winter storms of concern.

3.3.3 Cloud optical thickness and effective particle radius

Finding the size of water droplets in the Park Range storms in areas affected and unaffected by the power plant emissions is the main purpose of using MODIS retrievals in this study. After determining a pixel is composed of liquid water cloud, or something close to it, using the cloud mask and cloud phase products, the effective particle radius (EPR) and cloud optical thickness (COT) products are examined. Fundamentally, EPR is defined as the ratio of the particle volume to the particle cross-sectional area in a droplet size spectrum. In mathematical terms; $r_e = \int r^3 n(r)dr / \int r^2 n(r)dr$ (Platnick et al., 2001). This measure is more easily retrieved from cloud reflectance than droplet radius and is used as a gauge of the droplet size distribution.

EPR and COT are retrieved simultaneously using the same reflectance measurements. Again, the absorption qualities of water make these retrievals possible. Due to the extremely small absorption by ice and water at the 0.85 micron nearby bands (0.65, 1.2 microns), these channels are useful for estimating the cloud optical depth (Wetzel, 1995). The reflectance data at these wavelengths are used in conjunction with reflectance at a MODIS water-absorbing band (1.6, 2.1, 3.7 microns) that is extremely sensitive to cloud

particle size (Platnick et al., 2001). To solve for the two unknowns, EPR and COT, the two reflectance measurements are compared with entries in a lookup table and matched with the combination of EPR and COT that give the best fit (King et al., 1997).

Unfortunately, the non-absorbing bands used to retrieve EPR and COT are influenced by surface albedo and, as mentioned in the cloud mask product summary, this means a snow-covered surface can contaminate cloud property estimations. Platnick et al. (2001) proposed using the 1.6 micron band reflectance as a surrogate for the traditional non-absorbing band over snow and ice surfaces. This method largely prevents snow surface contamination but also increases the EPR and COT calculation sensitivity to measurement error. Operationally, the 1.2 micron band is used to gain optical thickness information while minimizing the surface albedo effect over snow/ice surfaces (Platnick et al., 2003).

Also of interest to this project is the related MODIS product water path (WP). Since the relationship between COT and EPR is dependent on WP, it is useful to compare effective radius measurements at a constant WP (Lohmann et al., 2000). The WP product is inferred from the retrieved EPR and COT and the mean extinction efficiency of the clouds (Li et al., 2005). These products are retrieved when ice as well as liquid water particles are present.

3.3.4 Cloud top temperature and pressure

Cloud top temperature (CTT) and pressure are determined using knowledge of partial infrared radiation absorption by carbon dioxide (CO_2). The absorption of upwelling infrared radiation in MODIS bands within the broad 15-micron CO_2 absorption region is sensitive to height in the atmosphere (Wylie and Menzel, 1999). Therefore, by measuring upwelling infrared radiation at the satellite for several MODIS CO_2 bands, the cloud top pressure can be inferred (Platnick et al., 2003). This technique is based on the assumption that all attenuation of upwelling radiation by clouds occurs at one level in the atmosphere, irrespective of variations in cloud density (Wylie and Menzel, 1999).

The MODIS CTT is estimated from global analyses of temperature and moisture from the National Center for Environmental Prediction (NCEP) (Menzel et al., 2002). Cloud top temperature and pressure products are generated for 5 by 5 pixel areas, or a 5km by 5km area at best.

3.4 SNOTEL and SPL measurements

While MODIS will be used to investigate possible aerosol effects on cloud microphysics, to judge variations in precipitation rate ground measurements are needed. To gain an understanding of possible effects of power plant emissions on regional snowfall requires many data points. Hourly precipitation data from 16 SNOTEL sites located in the Park Range were used to meet this need. The quality and limitations of SNOTEL reports are

discussed below. Additionally, an overview of SPL instruments and measurement techniques relevant to this study will be given.

3.4.1 SNOTEL observation system

More than 700 SNOTEL sites collect snowfall and precipitation data in 11 western U.S. states. Sites in Colorado are well located for the purposes of this study. The instruments were originally placed in heavy snow accumulation regions and at locations important for regional hydrology management. In general, this means many SNOTEL sites dot mountainous regions in western states, including the Park Range. A map of the positions of SNOTEL sites utilized in this study is shown in figure 3.6 with the approximate locations of the towns of Craig and Hayden added for reference. Table 3.1 gives the names of the 16 SNOTEL sites used in this study as well as their exact location and elevation. These sites lie in the mountains, mainly to the west and south and typically downwind of the Craig and Hayden power plants.

In the course of their study of Colorado snowpack climatology, Serreze et al. (1999) reported on SNOTEL data quality and some instrument limitations. They also provided a detailed technical description of the SNOTEL instrument operation, much of which will be paraphrased here. They write that SNOTEL stations are fully automated and unattended. A fact that has been the source of some concerns regarding data quality according to Doesken and Schaefer (1987) (as cited by Serreze et al., 1999). Snow water

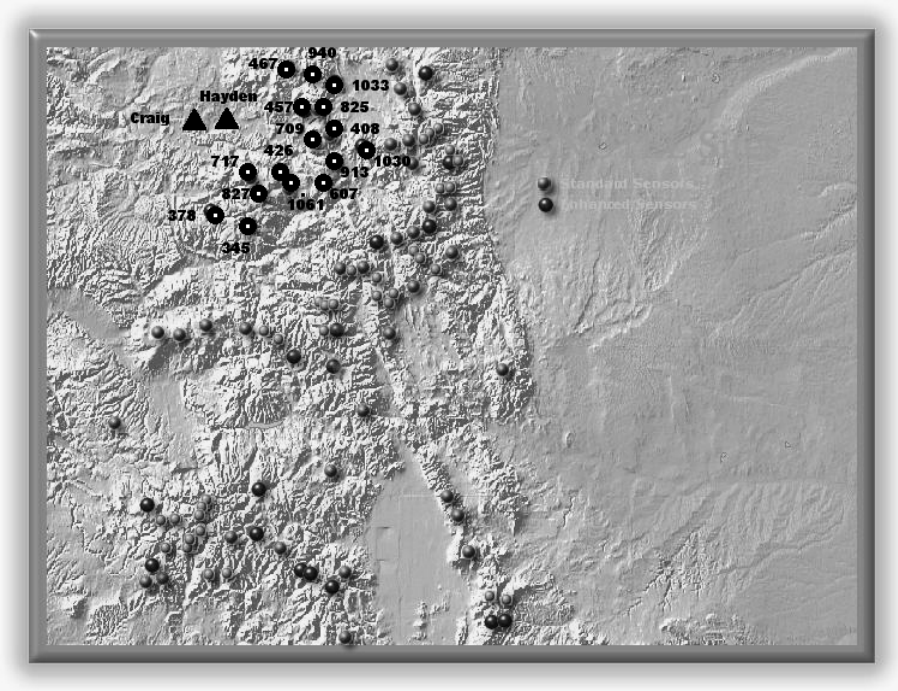

Figure 3.6: A map of Colorado showing the locations of the 16 SNOTEL sites used in this study. The locations of the Craig and Hayden power plants are shown for reference. (Source: http://www.wcc.nrcs.usda.gov/snow/)

SNOTEL site	ID #	Latitude (˚N)	Longitude(˚W)	Elevation (m)
Elk River	467	40.847812	106.968707	2676.9
Lost Dog	940	40.815883	106.748350	2867.7
Zirkel	1033	40.794883	106.595350	2873.8
Dry Lake	457	40.533972	106.781296	2584.6
Tower	825	40.537427	106.676797	3230.8
Columbine	408	40.394798	106.604077	2818.5
Rabbit Ears	709	40.367826	106.740376	2892.3
Arapaho Ridge	1030	40.350983	106.381416	3372.3
Buffalo Park	913	40.228611	106.595277	2843.1
Crosho	426	40.167454	107.057499	2800.0
Lynx Pass	607	40.078055	106.670277	2732.3
Bear River	1061	40.061533	107.009550	2793.8
Ripple Creek	717	40.108123	107.294113	3181.5
Trapper Lake	827	39.998839	107.236198	2984.6
Burro Mountain	378	39.875050	107.598533	2892.3
Bison Lake	345	39.764865	107.356812	3347.7

Table 3.1: A list of the 16 SNOTEL sites used in this study with names, ID numbers, latitude, longitude and elevation. (Source: http://www.wcc.nrcs.usda.gov/snow/)

equivalent (SWE) measurements are made using snow pillows filled with an antifreeze solution, as described by Serreze et al. (1999). Accumulating snow displaces the antifreeze solution, driving it into a manometer column. The weight of the fluid column is representative of the accumulated SWE and is monitored automatically every hour. Also explained by Serreze et al. (1999) are the SNOTEL precipitation gauge attributes. The gauges are located inside an Alter wind shield to minimize the effects of wind on precipitation collection. Each gauge stores precipitation for one year and is measured, just as the SWE, by weight. The instruments are powered by solar-charged batteries.

Serreze et al. (1999) bring to light several limitations of SNOTEL data that are important for interpretation of the data presented on the Park Range in the current study. To begin with, it has been observed that small precipitation events do not always correspond with increases in SWE and an increase in SWE is not always reflected in a corresponding precipitation event. Furthermore, cumulative precipitation and SWE values decline slightly on occasion, an error that is attributed to the formation of snow bridges above the snow pillow device (Serreze et al., 1999). The snow bridging may also lead to problems with snow event timing. Snow builds up on the snow bridge, preventing snow event measurement, and eventually collapses causing a recorded precipitation event at some time after the snow fell. These errors are of concern to the current work because for small precipitation events, instrument error may create variations in precipitation rates and event timing on a similar scale to the meteorological variability of interest.

Overall, Serreze et al. (1999) found nearly all (72 out of 75) SNOTEL sites recorded SWE within 15% of co-located human observations without under or over-measurement bias for one month of record. While errors must be considered when interpreting the data, the time resolution of the data and the site locations make the SNOTEL system an obvious data source for this study.

3.4.2 SPL instruments and data

The Storm Peak Laboratory, operated by the University of Nevada's Desert Research Institute (DRI), records valuable, long-term information about cloud microphysics and atmospheric chemistry at an elevation of 3210m above sea level near Steamboat Springs, CO (Borys and Wetzel, 1997). Its height and mountain-summit location allows for measurements of free tropospheric air and also makes it an ideal lab for the study of orographic clouds. SPL is often enveloped in clouds in the winter months permitting frequent in-cloud measurements of cloud microphysics.

Instruments have been installed at SPL to monitor many aspects of the atmosphere. To measure the liquid water droplet size distribution that is of interest for this study, the PMS-FSSP-100 (Forward Scattering Spectrometer Probe) is used. The FSSP samples droplet sizes for 15 minutes and reports the concentration of cloud droplets in 40 separate size bins ranging from about 2 to 47 microns. It is mounted on a wind vane to orient the air intake into the wind (Borys et al., 2000). Data from this instrument are not continuous and, for this study, were only available for the February 12th case. Measurements of

snowfall rate from SPL were also used in this study to supplement the SNOTEL data. Mean snowfall rate was estimated with output from a heated tipping-bucket precipitation gauge.

Data from these sources are used to examine differences between assumed CCN-rich and CCN-clean environments. The next chapter will explain how these two environments are distinguished from one another using simulations of the Craig and Hayden power plant emissions.

Chapter 4 - Model Simulations

In the absence of direct measurements of CCN a method for estimating the distribution of CCN concentration is needed. Once such method, as used by Harshvarden et al. (2002), is to model anthropogenic aerosol emissions and use the resulting aerosol concentration estimates as an indicator of high CCN areas. Past work has shown that CCN concentrations in the plumes of isolated coal-fired power plants are, in general, considerably higher than concentrations in the ambient atmosphere. If the approximate location of the emission plume is calculated, it can be reasonably assumed that the in-plume region is CCN-rich compared to the ambient air.

The diffusion of the Craig and Hayden plumes was simulated by calculating particle trajectories with a Lagrangian particle dispersion (LPD) model. Meteorological output used in these simulations was produced with the Regional Atmospheric Modeling System (RAMS) (Cotton et al., 2003). After the particle trajectories were analyzed, particle concentrations were computed and used to designate an "in-plume" region and an "ambient air" region. Details of the RAMS and LPD setup and use will be given in this chapter, as well as a thorough description of the representation of effective stack height (ESH) in the LPD model. Since the RAMS model output was not analyzed in this study but used as input for the dispersion model, the model structure and physics will not be discussed in detail. Finally, the results of the simulations will be presented and discussed in section 4.4.

4.1 RAMS setup

A recent version of RAMS, version 4.3, was used in this study and is described in detail by Cotton et al. (2003). This versatile numerical prediction model was convenient for this study because it was developed at Colorado State University (CSU) and because RAMS output is compatible with the LPD code.

The region of interest for this project is about 340 km by 330 km - much smaller than the state of Colorado. But the meteorological processes that will affect the plume dispersion in the study area take place on a larger scale. Thus, large-scale simulations are necessary. RAMS has a multiple grid nesting scheme that permits it to model the atmosphere on any number of interacting data grids with differing spatial resolution (Cotton et al., 2003). The multiple nested grid system allows for the inclusion of synoptic scale atmospheric processes in the simulation while retaining the option of high-resolution forecasts over the study region. The four case studies were simulated on a three-grid system. The sizes and arrangement of these grids are shown in Figure 4.1.

The outer grid (grid 1) covers most of the contiguous United States with 100 X 74 grid points at a spatial resolution of 48km. Grid 2 is nested within this area and has 78 X 74 grid points at a resolution of 12km. Grid 3 encloses roughly the previously defined study area, centered near Steamboat Springs, Colorado, and will provide the meteorological output for use by the dispersion model. At a grid spacing of 3 km (118 X 110 grid points) this grid offers the desired detail for the emission plume simulation.

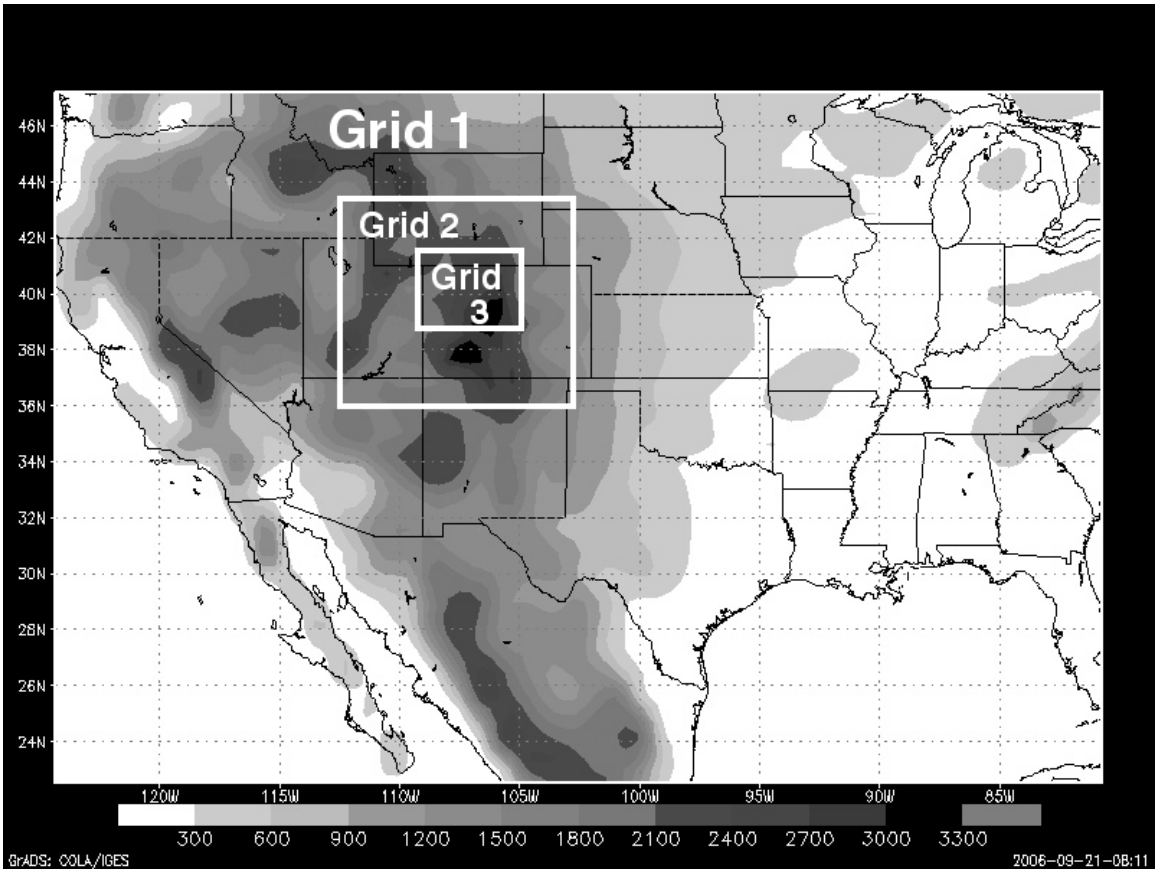

Figure 4.1: RAMS grid configuration with the outer grid (Grid 1) encompassing the whole map. Topography is overlaid in meters.

RAMS uses the terrain-following sigma-z vertical coordinate system. For these runs the model was set up with 40 vertical levels with a vertical grid spacing of 75m at the surface. This grid spacing is stretched by a factor of 1.12 with each increasing vertical level reaching a maximum of 750m grid spacing. In this way the model provides detailed output in the boundary layer but also represents the upper troposphere. The model time steps are 60s, 20s and 6.67s for grids 1, 2 and 3 respectively. Eddy viscosity was represented in the horizontal plane using Smagorinsky (1963) and in the vertical by the

level-2.5 prognostic turbulent kinetic energy (TKE) closure scheme of Mellor and Yamada (1982). The quantity and distribution of TKE output in the simulation will directly affect the dispersion of particles in the LPD. See Table 4.1 for details of the model physics and boundary schemes.

Model Aspect	**Setting**
Microphysics	Two-moment bulk microphysics - Meyers et al. (1997) Includes cloud water, rain, pristine ice, snow, aggregates, graupel, hail
Turbulence scheme	Horiz. diffusion parameterized according to Smagorinsky (1963) Vertical diffusion based on Mellor and Yamada (1982) scheme
Radiation scheme	Two-stream parameterization developed by Harrington (1997)
Lateral boundary	Klemp and Wilhemson (1978) radiative boundary
Surface boundary	LEAF-2 scheme - Walko et al. (2000)

Table 4.1: Chart of model physics options used for all four simulations.

Since grid 3 is about 340 km by 330 km and initially no particles will be present in the dispersion model run, the simulation period must be long enough to allow the power plant plumes to disperse throughout the study area. All four simulations were begun at 1200Z on the day prior to the case study storm (see Table 4.2 for model run times). For example, the February 12th model run began at 1200Z on February 11th. With the storms being scrutinized at around 1800Z, this gives approximately 30 hours of model spin-up before in-plume areas need to be identified. All four RAMS runs were carried out for 36 hours.

Case study	Start time	End time	Total time
12-Feb	1200Z February 11	0000Z February 13	36:00:00
15-Feb	1200Z February 14	0000Z February 16	36:00:00
19-Feb	1200Z February 18	0000Z February 20	36:00:00
22-Feb	1200Z February 21	0000Z February 23	36:00:00

Table 4.2: Chart of model start time, end time and total running time for all four cases.

RAMS was initialized using the NARR dataset mentioned in Chapter 3. NARR data are available at 3-hour intervals from 1979 to the present. Being a reanalysis, the dataset is created using the 3-hour forecast from the previous cycle as the first guess for the next cycle (Mesinger et al., 2006). Observations are assimilated from various sources from rain gauges to satellite retrievals to improve the meteorological fields. NARR data has a horizontal resolution of 32 km and 45 layers in the vertical (Meisnger et al., 2006). NARR data was also used to "nudge" the lateral boundaries of grid 1 every 3 hours during the simulations. To some extent, this constrains the model to observations while it's running.

4.2 Mesoscale dispersion modeling system (MDMS) and LPD

The next step in the emissions forecast is to calculate particle dispersion from the power plant sources. The Lagrangian particle dispersion model, in short, makes possible the simulation of release of particles from arbitrary sources by tracking the motion of the particles (Uliasz, 1993). This model code was developed at the Warsaw University of Technology in Poland as part of the mesoscale dispersion modeling system (MDMS) described by Uliasz (1993) and Uliasz and Pielke (1990).

The LPD ingests the wind field, temperature field and TKE output from RAMS to determine the movement of particles. The LPD can track particles forward in time or backward in time. This study is concerned with forward trajectories that will represent the plume evolution from the emission sources. Particles are moved by the wind, both horizontally and vertically, and by a sub-grid scale turbulent velocity component. The turbulent velocity is calculated with a Markov-chain scheme in which a particle's turbulent movement depends on the turbulent velocity at the previous time step and on a random component (Uliasz, 1993). Dry deposition of particles onto the ground surface is included in the LPD runs with an absorption probability calculated following Monin (1959) and Boughten et al. (1987) (as cited by Uliasz, 1993).

Once particle trajectories have been calculated for the time period in question, supplemental code is utilized to compute grid-box concentrations of the particles. This code includes up to five model output files and produces a time-averaged concentration field. The purpose of taking a time-average is to smooth out the random particle locations present in a single time frame.

The LPD was setup to run for the same 36-hour periods as the RAMS simulations and cover the same area as grid 3, which was the exclusive meteorological data source. Five emissions sources were defined. These represent the three coal-firing units in operation at the Craig power station and the two units at the Hayden power station. Each of these units has its own emission stack and a unique rate of sulfur dioxide and NOx emissions.

All five units operate 24 hours but are periodically shut down for maintenance. During these four case studies there were no unit shut downs, but the emission rate at all units fluctuated. Table 4.3 shows the sulfur dioxide rates for all five units averaged over each 36-hour case study period.

		SO2 rate (lbs/hr)		
Coal-firing Unit	**Sim 1**	**Sim 2**	**Sim 3**	**Sim 4**
Craig 1	119.6	163.9	253.5	266.2
Craig 2	160.4	174.5	246.8	240.2
Craig 3	517.3	544.7	676.3	611.1
Hayden 1	304	305.5	316.4	328
Hayden 2	364.2	353.3	379.9	351.9

Table 4.3: Average rate of sulfur dioxide emission during each simulation for all five coal-firing units. Data have units of lbs/hr of sulfur dioxide. (Source: Environmental Protection Agency (EPA) - http://www.epa.gov/airmarkets/emissions/raw/index.html)

The emission rates of all units were represented relative to one another in the LPD. This was done by setting up the model to emit a number of particles proportional to the average emission rate (Table 4.3) each time step. For example, Craig unit 1 emitted 1.20 particles per time step during the February 12th case compared to 1.60 particles for Craig unit 2 for the same period. By this method the comparatively large sulfur dioxide emissions of Craig unit 3 during this case and the unique emission rates of all the units are accounted for.

As mentioned before, these power plants emit large amounts of NOx as well as sulfur dioxide. Since sulfur dioxide typically leads to larger CCN amounts than NOx, especially in environments low in sea-salt aerosol, only the sulfur emissions will be included in the model setup. This way the forecast concentration of particles will presumably be more

proportional to CCN amounts than gaseous particle emission amounts. Information about unit location and stack qualities that was used in the LPD simulations is given in Table 4.4. Note that not only does the source location vary horizontally but also in the vertical, given the different stack heights and stack qualities. The source height issue is discussed in detail in the next section.

Unit	Latitude	Longitude	Stack height	Stack Temp	Stack Diameter	Effluent Velocity
	(degrees)	(degrees)	(meters)	(Kelvin)	(meters)	(m/s)
Craig 1	40.4644	-107.5902	185	316.48	8.67	12.62
Craig 2	40.4644	-107.5902	185	316.48	8.67	12.92
Craig 3	40.4644	-107.5902	185	348.71	7.70	17.23
Hayden 1	40.4867	-107.2035	77	350.37	6.0	7.13
Hayden 2	40.4871	-107.1798	121.5	345.93	6.5	7.37

Table 4.4: Information about the five coal-firing units used as sources in the model simulations. Listed are the latitude and longitude, the stack height (meters), the average stack temperature (Kelvin), the stack diameter (meters) and the effluent velocity (m/s). (Source: Chad Campbell and Dana Stevens, personal communications, 2006)

4.3 Particle source height representation

The air mass emitted from industrial stacks, called the effluent, typically enters the atmosphere at a high temperature relative to the ambient air. Some short-stack industrial sources have effluent temperatures well in excess of 400K (Stocker et al., 1992). The potentially large temperature difference between the effluent and the ambient air causes the effluent to be positively buoyant as it exits the stack. This initial buoyancy is accounted for in the LPD by using an "effective stack height" (ESH) in place of the physical stack height. The ESH is, essentially, an estimate of the change in height a plume will gain due to its initial buoyancy. Since coal-fired power plant stacks are

typically much hotter than their environment, using the ESH will increase the height of emission. Briggs (1975), in a thorough summary and analysis of plume rise prediction work, wrote that this buoyancy leads to an ESH that's more than twice the actual source height whenever the wind is less than 10 m/s, which is most of the time. Some industrial stacks have ESH values computed up to 1 km and for some atmospheric conditions the ESH may be as large as ten times the height of the actual stack (Briggs, 1975).

Depending on the local wind and temperature profile, a two-fold or more change in stack height could cause a drastic change in the final destination of emitted particles. Recall Rauber and Grant's (1986) observation that inversions commonly cover much of the valley region that contains Craig and Hayden during the winter. In the event of such an inversion, the ESH of the Craig and Hayden power plants may be high enough to inject aerosol into the atmosphere above the inversion. Meanwhile many surface aerosol sources may be cut off from the mid-upper troposphere, strengthening the influence of the power plant emissions on the middle atmospheric aerosol burden.

4.3.1 Sensitivity of plume dispersion to source height

To illustrate the possible influence of plume buoyancy on the dispersion of particles in that plume, a sensitivity study was carried out. A description of the different cases can be found in Table 4.5. Figure 4.2 displays the concentration of particles averaged from 22:00Z on February 11th, to 00:00Z on February 12th for Case 1. Note the general movement of particles to the southeast in the areas of highest concentration.

Sensitivity study case descriptions	
Case 1	Source height equal to the physical height of the stacks
Case 2	Source height equal to twice the physical height of the stacks
Case 3	Source height equal to 5 times the physical height of the stacks
Case 4	Source height of all stacks equal to 5 times the height of the Craig stacks

Table 4.5: Descriptions of how the source height was varied for each of the four sensitivity study cases.

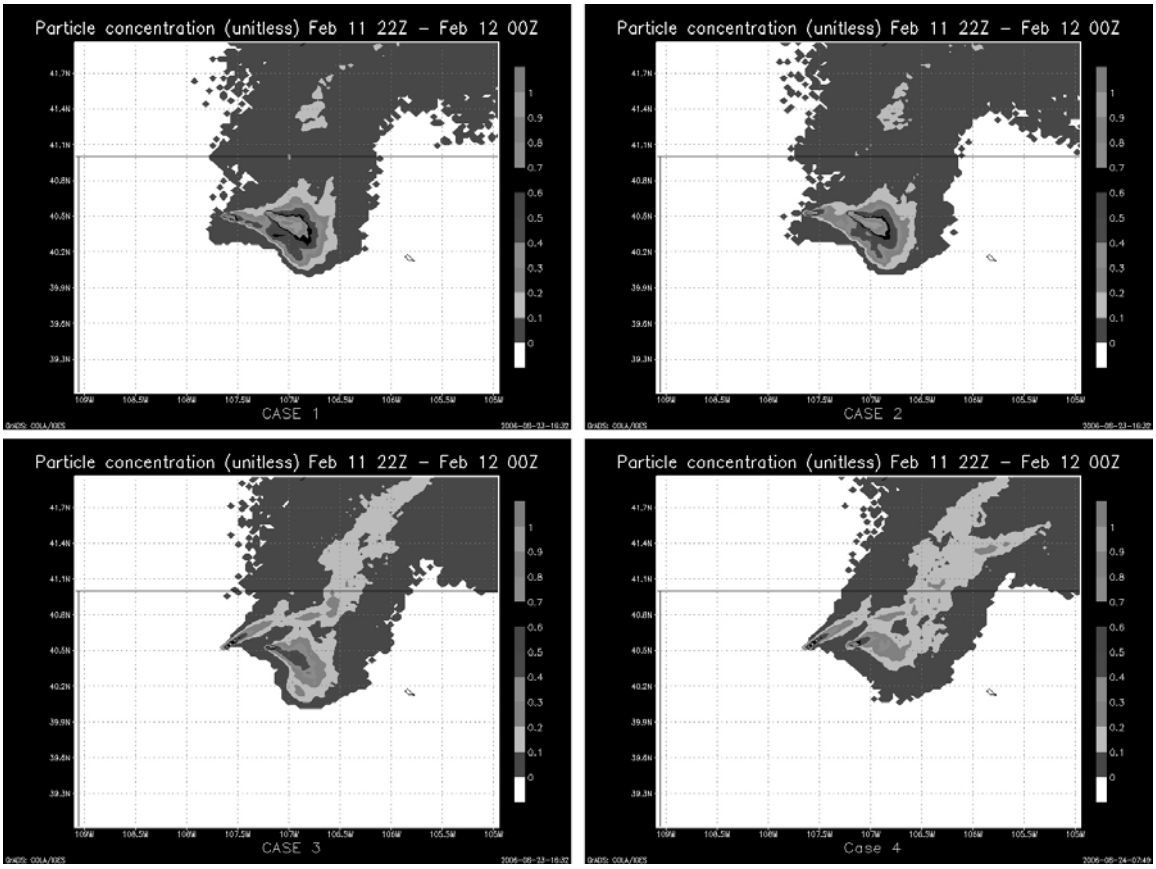

Figure 4.2: Total column (0-10km) particle concentration averaged from 22:00Z February 11, to 00:00Z February 12 for all four sensitivity study cases – Case 1 (top left), Case 2 (top right), Case 3 (bottom left), and Case 4 (bottom right).

Concentrations are high in these areas near the sources because particles haven't had time to diffuse to a great extent. Therefore the southeast particle movement is likely indicative

of northwest wind in the lower levels of the atmosphere. Older particles have dispersed to the north and east.

Differences between Cases 1 and 2 are very minor (see Figure 4.2). The initial plume direction has shifted due east for the Craig plume and remained similar for Hayden. The plume area coverage remained very comparable to Case 1. More divergence from Case 1 was expected because past work has noted that plume dispersion is very sensitive to the ESH (Schatzmann and Policastro, 1984; Hanna, 1972).

Case 3 showed more divergence from the previous two examples, though admittedly the 5X stack height ESH lies at the high end of expected ESH values. The Craig emissions are taken straight to the northeast upon release, oriented with the mid-atmospheric winds. Larger concentrations extend well to the north and the coverage of the Craig and Hayden plume has shifted to the east. While an ESH of 5X the stack height may be unusually high, the work summarized by Brigg (1975) suggests it's not out of the question. The changes caused by raising the ESH to this height are significant and demonstrate the need to account for the ESH in the model.

Curiously, the high concentrations protruding from the location of Hayden still flow generally southeast in Case 3. Since the Hayden stacks are much shorter than those at Craig, a factor of 5 may not be enough to extend the Hayden ESH into the southwesterly flow. But as is typical with shorter stacks, the effluent temperature is high in the Hayden units that may lead to high ESH's similar to those at Craig. When all the release heights

are set to the 5X Craig height in Case 4 (Figure 4.2), the Hayden plume initially extends into the northeast just as the Craig plume does.

All these images show particles totaled from the surface to 10km, but the release height influences concentrations within thinner layers. As a brief example of this, Figure 4.3 shows particle concentrations in the layer between 2km and 3km above the surface for Case 1 and Case 3 conditions on February 14th 23:00Z to February 15th 00:00Z. Concentrations are much higher and located farther south when the model is initialized with Case 3 conditions. This adds to the case for using the more realistic ESH release height in the LPD instead of the physical stack height.

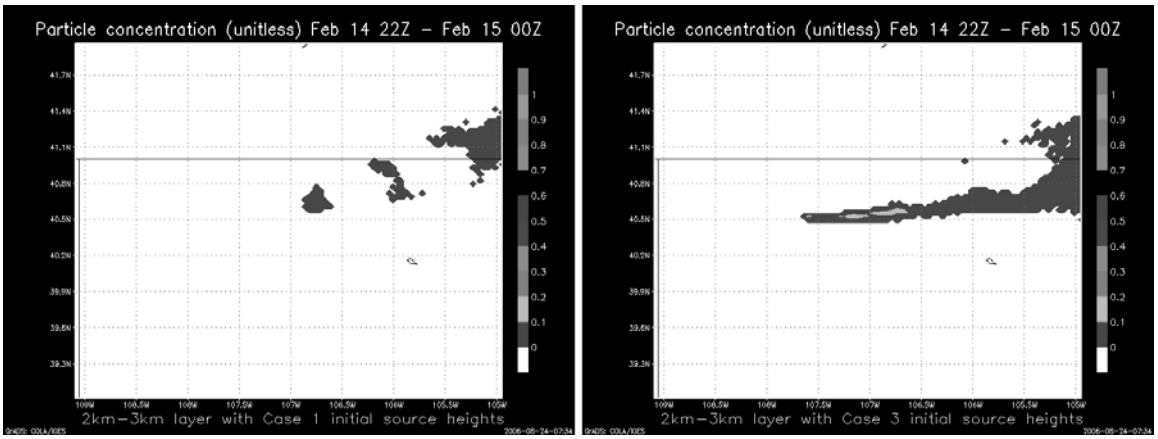

Figure 4.3: 2-3km layer particle concentration averaged for 22:00Z February 14 to 00:00Z February 15. Source height the same as in sensitivity study Case 1 (left) and Case 3 (right).

4.3.2 Calculation of ESH in LPD

The results of the sensitivity study demonstrate the need to emit particles from an ESH in these simulations. As might be expected, the ambient temperature and stability of the lower levels of the atmosphere impact the rise of the plume and thus, affect the ESH used in the model. During stable atmospheric conditions, a plume will rise steadily and level off, as observed by Briggs (1975). However, in neutral or unstable conditions, the plume will act quite differently, rising quickly and chaotically and not leveling off (Briggs, 1975). The ambient temperature and stability vary with time requiring that the ESH be calculated continuously throughout the simulation. The calculation of ESH was added to the LPD code and follows the method laid out by Briggs (1975) that will be described here.

To represent the different plume rise characteristics during stable conditions and during neutral or unstable conditions, two equations are employed. The use of one or the other of these equations is determined by the sign of the static stability ($d\Theta/dZ$) of the lowest kilometer of the atmosphere. In the case of a positive static stability (stable atmosphere) the following equation was used to calculate the ESH:

$$H_e = H_s + 2.6*(F/U_s)^{1/3}$$

Where H_e equals the ESH, H_s is the actual stack height, U_s is the wind speed at the source height and F is defined as the "buoyancy flux". The buoyancy flux is a function of the

temperature difference between the effluent and ambient air, and the initial volume flux of the effluent through the stack. The data used to calculate the buoyancy flux can be found in Table 4.4.

Stable conditions were most common for the four case studies used here but in the event of neutral or unstable conditions in the lower 1km of the atmosphere, this alternate formula was implemented:

$$H_e = H_s + 1.54*(F/(U*u^2))^{2/3}*H_s^{1/3}$$

The variable "u" in this case refers to the friction velocity. Values for "u" were provided for a "mixed countryside" land type by Briggs (1975). This equation takes into account the tendency for plumes to "break-up" due to ambient turbulence in a neutral or unstable layer.

In the dispersion model, particles are emitted from the ESH with initial temperature and velocity equal to that of the ambient atmosphere, not influenced by the stack physics. Using this approach, the ESH of the Craig and Hayden units typically falls between 100m and 500m above the physical stack height. It may be of interest to compare the particle concentration for February 11th 22:00Z to Febraury 12th 00:00Z using the ESH to the images from the sensitivity study (Figure 4.4). The plume dispersion character seems to lie somewhere in between cases 1 and 3 which is reasonable in light of the typical calculated ESH values.

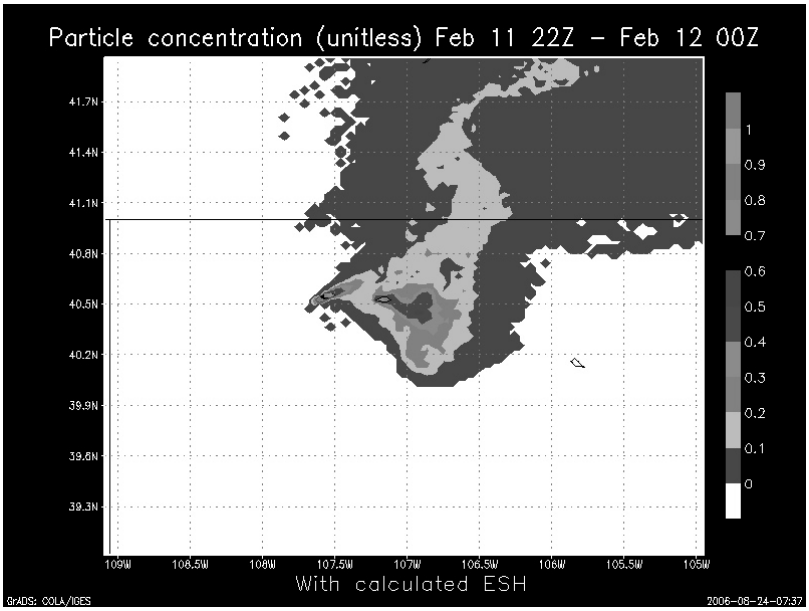

Figure 4.4: Particle concentration for the 0-10km column averaged from 22:00Z February 11 to 00:00Z February 12 using the model calculated ESH.

The buoyancy flux used in these formulas does not take moisture influences into account. Often times, due to the wet scrubbing processes used in power plant stacks to clean up emissions, the effluent can carry large amounts of moisture into the ambient atmosphere. A moist plume might saturate during its ascent, releasing latent heat due to condensation and altering the buoyancy of the plume. Schatzmann and Policastro (1984) go so far as to conclude that dry plume rise equations are "inappropriate" for describing emissions from stacks with wet scrubbers (Craig units 1 and 2 use wet scrubber systems). Hanna (1972) also suggest including a latent heat release term in the calculation of plume buoyancy. Unfortunately, effluent moisture content data were not available for these cases. It is therefore likely that the calculated ESH values are underestimates in many instances.

4.4 Model output

In this section, the model output from all four case studies will be presented and used for its original purpose – to provide an estimate of regions of high CCN and low ambient CCN concentrations. High CCN concentrations are presumed to exist within the area of the study region under the power plant plume, an area distinguished as "in-plume". The "ambient air" territory, outside the influence of the power plant plume, is assumed to contain lesser concentrations of CCN. The ambient air zone will generally include the area inside 108˚W and 106˚W, and 39.5˚N to 41˚N, excluding the in-plume area and any part of the box not affected by the winter storm. The ambient air zone may be extended to include more winter storm-influenced areas in an attempt to increase the amount of data for analysis in this zone.

The particle concentrations for all case studies are column totals from heights of 0km to 10km and averaged from 17:00Z to 19:00Z on the winter storm date. Individual layer concentrations will be analyzed when relevant in Chapter 5. Limiting the analysis to this time period causes problems when observing a time-varying entity such as a winter storm. But this way the model output will be lined up with the overpass of the MODIS instrument, a major observation tool for this study. The same particle concentration scale was used for all model output images.

It is important to note when viewing the model images that the concentrations in the LPD output are unitless. The concentrations are proportional to the amount of emitted SO_2 but do not represent the amount of SO_2 or sulfate in the atmosphere. The amount of SO_2 represented by each particle could be calculated knowing the initial SO_2 emissions rates, but this does not take into account the many atmospheric sources and sinks of SO_2. Dry deposition is included in the model simulations, but the processes of wet deposition, gas to particle conversion, and scavenging are not represented.

A concentration of 0.05 and above was used to outline the in-plume region. Since the model output concentration is not a representation of CCN concentration, the 0.05 threshold was determined using plume measurements from Hobbs et al. (1980) and Mamane and Pueschel (1980). Both studies found in-plume CCN or condensation nuclei (CN) concentrations to be about an order of magnitude greater than in the ambient air. Mamane and Pueschel (1980) mark the boundary of the measured plume as the line for which CN concentration is approximately 5% of the greatest CN concentration measured in-plume.

On February 12, the Craig and Hayden emissions were transported nearly due east over the Park Range (Figure 4.5). High concentrations extend well downwind but are highest in the vicinity of the sources. Small numbers of particles escaped the straight west wind and were carried northward. Even fewer particles went south of the main flow. The in-plume region for this case includes SPL as well as the northern SNOTEL stations and extends north into Wyoming (Figure 4.6).

The case of February 15th appears similar to that of the 12th at first glance (Figure 4.5). The plume stretched eastwards out from the sources but the main particle stream turned slightly north after reaching the Park Range high peaks. Synoptic maps from this case indicate very high winds aloft (see Figure 3.3). The high winds may have been responsible for the advection of particles away from the sources and out of the study region quickly, accounting for the lower concentrations and minimal diffusion during this

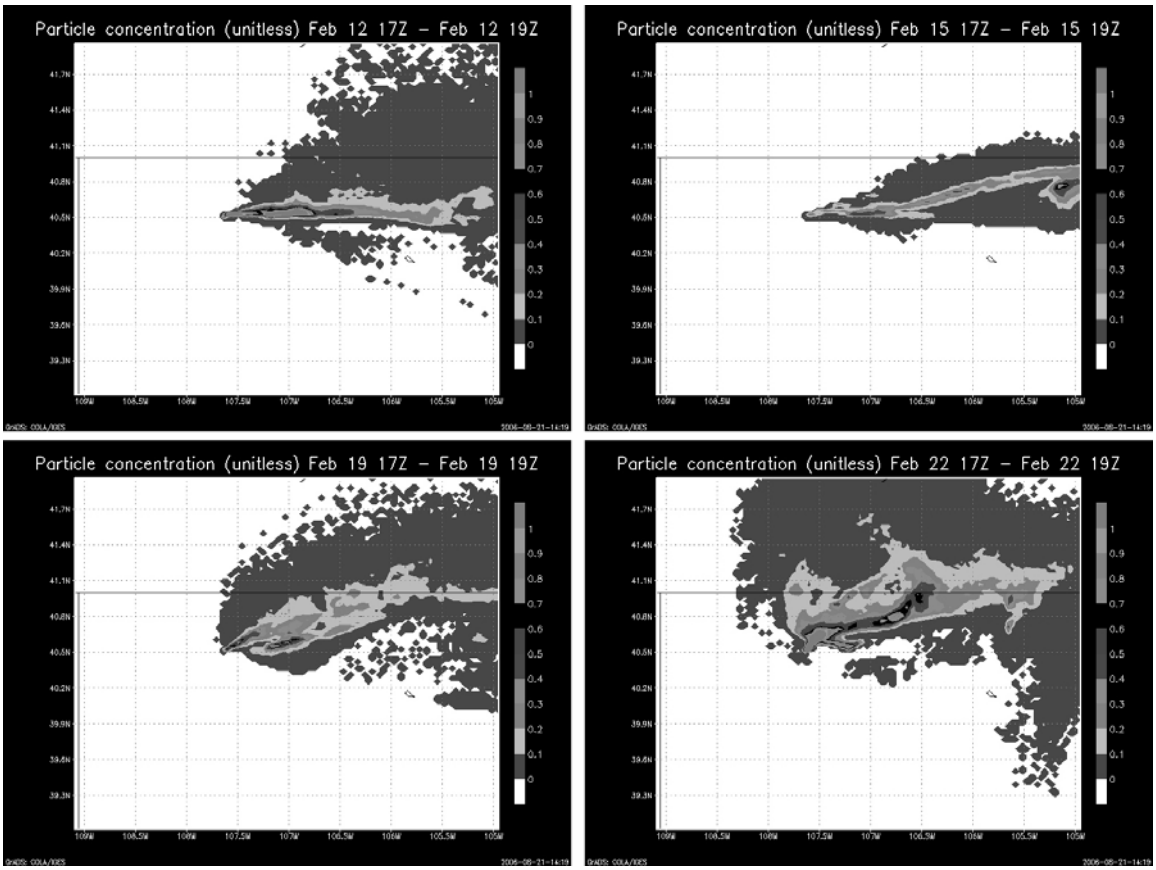

Figure 4.5: Particle concentration for the 0-10km layer averaged from 17:00Z to 19:00Z on each of the four winter storm case dates – February 12 (top left), February 15 (top right), February 19 (bottom left), and February 22 (bottom right).

period. The in-plume region includes the low concentrations to the north and south of the main particle flow, though the location of the main flow will not be forgotten (Figure 4.6).

February 19th saw generally northeast motion of particles (Figure 4.5, Figure 4.6). The highest concentrations were located near the power plants and particle number decreased with distance away from the sources. A large swath of low concentrations surrounded the main drift of particles and covered greater area to the north of the flow. The plume

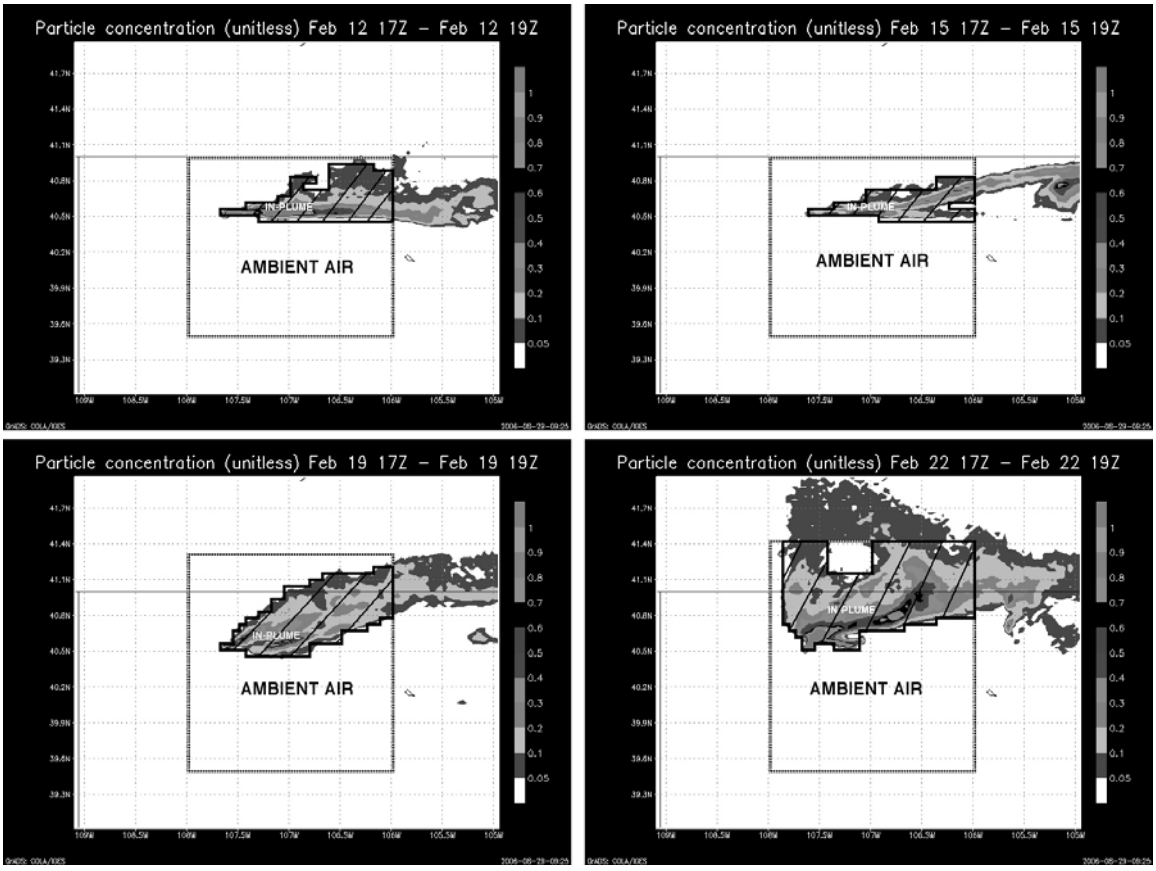

Figure 4.6: Same as in Figure 4.5 except only particle concentrations over 0.05 are marked. The hatched area represents the in-plume region and the remaining area in the box labeled "ambient air" is the ambient air region for - February 12 (top left), February 15 (top right), February 19 (bottom left), and February 22 (bottom right).

seemed to extend southwards east of 105.5˚W, or along the Front Range. This southern extension will not be included in the in-plume region since it is well outside the extent of the snowfall in this case.

The storm of February 22nd also moved the power plant emissions generally to the east (Figure 4.5). Rauber and Grant's (1986) contention that most winter storms over the Park Range can be characterized as westerly wind events certainly holds for these four cases. However, the deviations from the eastward flow in this case are worthy of note. While high particle concentrations emitted from the Craig units initially flow northeastward, at Hayden the particles acquired westward momentum out of the stack. This could have been caused by a height differential between the high Craig ESH values and lower Hayden release points and a wind that veered with height. High concentrations extended well east of the Park Range and also to the north. A similar southward extension along the Front Range appears on this date as well. The ambient air zone was extended for this case to increase the amount of data included (Figure 4.6).

The dispersion model runs resulted in similar in-plume areas for all four cases. If an aerosol effect on precipitation is found in this study, and these storms can be considered representative of the local climatology, the existence of a long-term aerosol effect in the northern Park Range should be studied. A recent study by Rosenfeld and Givati (2006) aimed to find a long-term effect of aerosols on precipitation in this region and in other western United States locations. They found a decreasing trend in precipitation upwind of Hayden during the winter for the Hayden-Steamboat Springs corridor, although the

last five years in the 50-year dataset were responsible for most of the trend. With in-plume and ambient air regions designated for this study, the satellite-retrieved cloud parameters and ground precipitation rate will be compared and contrasted for both regions to see if an aerosol effect on precipitation can be found on a case study basis.

Chapter 5 - Results and analysis

The four storm cases from February 2005 took place in various synoptic weather arrangements but resulted in similar particle dispersion output. The environment at cloud-top and the precipitation rate at the surface will now be considered for the in-plume and ambient air regions. Analysis of the MODIS data will be discussed first. Based on previous measurements summarized in Chapter 2, it is expected that in-plume clouds will exhibit lower EPR's relative to clouds in the ambient air regions. Though, several difficulties arise when attempting to characterize continental clouds with cloud-top reflectance measurements. These will be discussed in section 5.1.

Secondly, the surface precipitation rate measured by the SNOTEL network and SPL will be introduced. In the presumably CCN-rich, in-plume regions, relatively low precipitation rates are anticipated. The observed signature of the local power plant emissions on the Park Range precipitation rate must be separable from synoptic and orographic effects to declare a visible aerosol influence. Finally, all results will be discussed in section 5.3. Each case will be considered in the context of the accompanying large-scale storm structure.

5.1 Analysis of MODIS data

Table 5.1 gives the time and swath location of the EOS *Terra* satellite overpass used to investigate the clouds for all four cases. The overpasses occurred between 17:15Z and

18:45Z and viewed a swath that included the entire study region. The MODIS-derived EPR observed during the four storms is shown in Figure 1. The locations of Craig, Hayden and SPL are given for reference.

Date	*Terra* Overpass	Approx. Swath Latitude (˚N)	Approx. Swath Longitude (˚W)
Feb. 12	18:15Z	32.980-54.466	124.64-89.94
Feb. 15	18:45Z	35.947-57.553	131.98-95.19
Feb. 19	18:20Z	36.725-58.380	125.69-88.28
Feb. 22	17:15Z	26.273-47.536	110.01-79.01

Table 5.1: EOS *Terra* satellite overpass times and approximate MODIS swath coverage for the four storm cases.

There is a striking contrast between particle size over the Colorado Rockies and the lower elevations to the west for the February 12 case (Figure 5.1). While a region of low EPR, around 10-15 microns, extends into the mountains at about 40.8˚N, the area within the model-forecasted emission plume exhibits slightly higher values of EPR. There doesn't appear to be a clear influence of the plume aerosol on the EPR in this image. Ice particles likely played a major role in the EPR measurements presented in this image. This hypothesis is supported by the MODIS cloud phase product for February 12, 1815Z (Figure 5.2). Cloud tops over the region to the west of the Park Range and to the east of the Front Range are largely glaciated. It is probable that the difference in particle radius between mountains and the western plateau was due primarily to differences in particle phase. The problem of abundant ice particles in these storms will be dealt with, to some extent, when pixel data values are analyzed in the next section.

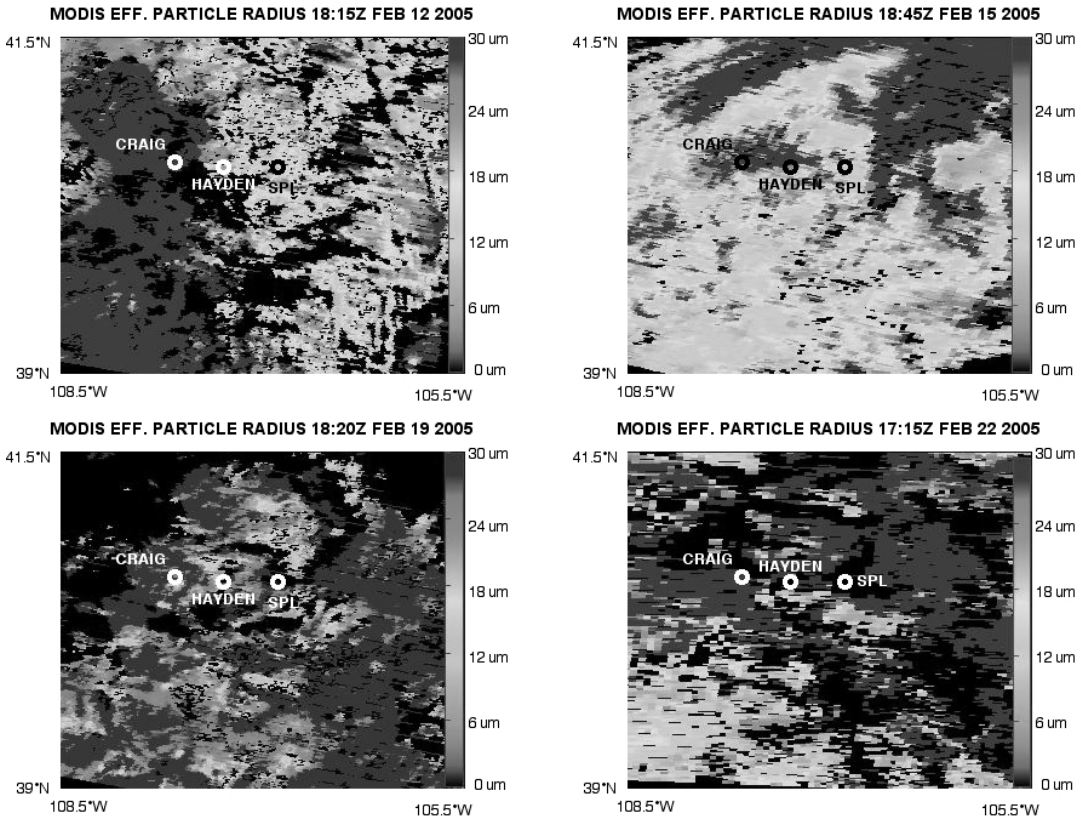

Figure 5.1: MODIS effective particle radius product for the study region for the February 12 case (top left), February 15 case (top right), February 19 case (bottom left), and February 22 case (bottom right). The locations of Craig, Hayden and SPL are marked for reference.

Data from the SPL FSSP instrument were available for the period encompassing the time of the MODIS overpass on February 12. The effective radius calculated from the FSSP droplet spectrum measurements at 18:17Z on February 12th was 12.9 microns. The largest concentrations of droplets were observed at radii of 10 microns and 13.5-14.5 microns. Compare this to a MODIS-derived EPR value of 17.14 microns, averaged over the 5km square pixel that included SPL. The FSSP measured droplet sizes were larger than the droplets observed by Borys et al. (2000, 2003) for the same location. They found droplet radii between 4 and 8 microns were typical. Unfortunately, FSSP data were available only for this case.

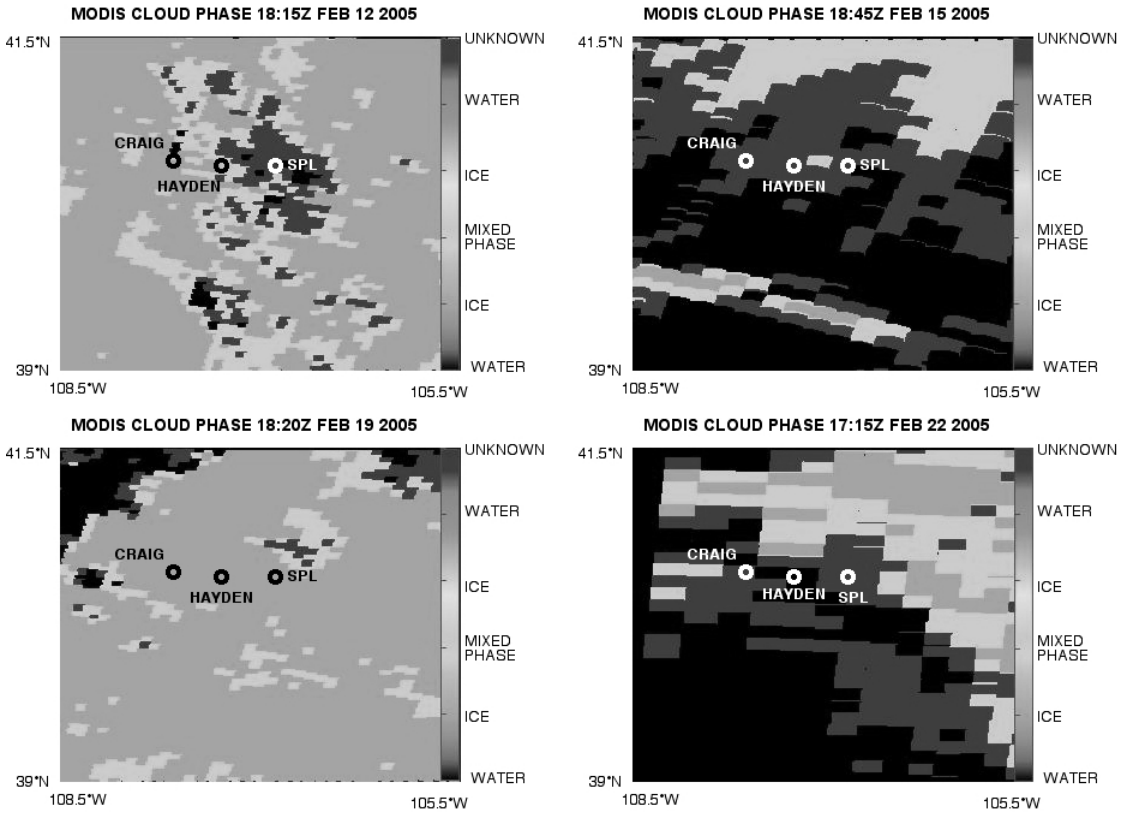

Figure 5.2: MODIS cloud phase product for the study region for the February 12 case (top left), February 15 case (top right), February 19 case (bottom left), and February 22 case (bottom right). The locations of Craig, Hayden and SPL are marked for reference.

The location of the power plant emission plume on February 15 was very similar to its location on February 12 as output by the LPD model (see Figure 4.5), but the EPR values for the region on these two dates were distributed very differently. On the 15th, the area surrounding Craig and Hayden was characterized by pockets of EPR values in the 12-18 micron range embedded in a zone of EPR's around 18-24 microns. The most striking feature apparent on this image is the sharp increase in EPR values over the Park Range, relative to areas to the west. The potent stream of power plant particles flows west to east, as predicted in Chapter 4, right through this region of large particle size. No clear

indication of a change in particle radius can be seen for this in-plume area. While the cloud phase product for this case suggests mainly liquid water in the northern Park Range, the phase was designated as "unknown" to the south (Figure 5.2). Therefore ice contamination cannot be ruled out as a factor in the observed high EPR values.

The EPR field at 18:20Z February 19 shows low values near the Craig and Hayden sources (Figure 5.1). This pocket of small particles is co-located with the area of highest predicted emission concentrations at this time. However, a quick glance at the cloud phase product for the February 19 overpass shows mainly ice phase pixels covering the study region. Small areas of mixed-phase pixels lie in the path of the plume.

A large percentage of cloud cover in the study region on February 22 was classified as liquid water or "unknown" (Figure 5.2). Unfortunately, the in-plume area cloudtops were mainly determined to be mixed-phase. The MODIS-retrieved liquid water regions to the south and east of the plume sources appear to correspond to the areas of lowest EPR values in the area (Figure 5.1). The in-plume region does not exhibit relatively low EPR values in this case. It appears to contain large areas of > 30 micron EPR and only small areas of EPR in the 12-18 micron range.

5.1.1 Pixel analysis method

The subjective glimpse into the cloud droplet size spectrums of clouds provided by Figures 5.1 and 5.2 does not give a clear indication of impacts on cloud microphysics by

the Craig and Hayden power plant emissions. Probable ice contamination in at least three of the four cases very likely masked any plume interaction with liquid droplets. Also, the vertical restriction of satellite retrievals of EPR to cloud tops undoubtedly limits the amount of cloud microphysics information provided by this MODIS product. This issue will be explored in section 5.1.2. To extract more quantitative results from the MODIS products, individual data pixels were grouped and analyzed for only the ambient air and in-plume regions. The method and results of this analysis are explained in this section.

Data pixels were separated into in-plume and ambient air classifications by latitude and longitude as derived from the dispersion model output. These data then underwent several checks and controls. First, products that are retrieved at 1km resolution were prepared to correspond to the 5km resolution data. Valid data points in 25-pixel squares of the 1km data were averaged, resulting in one value that roughly corresponded in latitude/longitude to a 5km data pixel. This alllowed for comparison of datasets at both resolutions.

Given that the four case studies are *winter* storms, they almost certainly contain mixed-phase clouds. The MODIS cloud phase product validates this speculation (see Figure 5.2). While the microphysics of ice particles is an important study, this project is mainly concerned with liquid particles. Some aerosol species, such as mineral dust, do act as ice nuclei (IN). Dust transport to the Park Range from distant sources can affect regional ice crystal numbers though it occurs most often in the spring and summer (DeMott et al., 2003). However, coal-fired power plant plume measurements by Hobbs et al. (1980) and

Schnell et al. (1976) found that coal combustion sources do not contribute statistically significant amounts of IN to the atmosphere.

MODIS measures cloud parameters, including effective particle radius, regardless of the determined phase of the pixel. To avoid incorporation of ice particle measurements where possible, the cloud phase product is used as a mask. All pixels deemed to consist of mainly ice particles by the MODIS cloud phase algorithm were flagged. Then, all cloud data from the locations of these flagged pixels was excluded. Those data co-located with a "mixed-phase" pixel were included for the February 12, 19 and 22 storms. The inclusion of these pixels was necessary to increase the number of valid data for these cases, but does ensure ice particles will be measured along with liquid water particles. Though, even in MODIS-designated "water" pixels, ice contamination is still possible.

Harshvardhan et al. (2002) noted that contamination of pixels by ice particles tends to result in abnormally high effective radius retrievals. Possible evidence of this effect was shown in Figures 5.1 and 5.2. Harshvardhan et al. (2002) set a limit of 30 microns on droplet size to eliminate measurements of ice particles. Platnick et al. (2003) report that the MODIS EPR algorithm does not calculate EPR values above 30 microns. They go on to explain that even EPR retrievals greater than 20 microns are problematic and are given less weighting in global studies. To follow the MODIS convention, a 30-micron effective radius limit was adopted for the four Park Range cases. All data pixels with EPR values over 30 microns were excluded.

5.1.2 Pixel analysis results

With these controls in place, frequency distributions of the EPR retrievals were generated for both in-plume and ambient air regions. Figure 5.3 compares the distribution of EPR in the inferred CCN-rich in-plume region to that of the inferred relatively clean surroundings for the February 12 case. The 14-16 micron size bin contains the greatest number of pixels in the in-plume region, while the peak frequency of EPR in the ambient air is larger – between 18 and 20 microns. The mean EPR for the in-plume region was 13.8 microns, compared to 15.1 microns for the ambient air region. The distribution is narrower for the in-plume region, meaning the number of pixels in size-bins above and below the peak drop off quickly. This does not necessarily mean the droplet size distribution was narrower for the in-plume region since EPR and not droplet radius is estimated by MODIS.

The frequency distributions of EPR retrievals for in-plume and ambient air regions on February 15 appear similar (Figure 5.4). Both distributions peak near 15 microns though the mean EPR for the in-plume region was slightly larger at 15.2 microns compared to 14.7 for the ambient air region. A large portion of the in-plume EPR values lie in the 20-30 micron range.

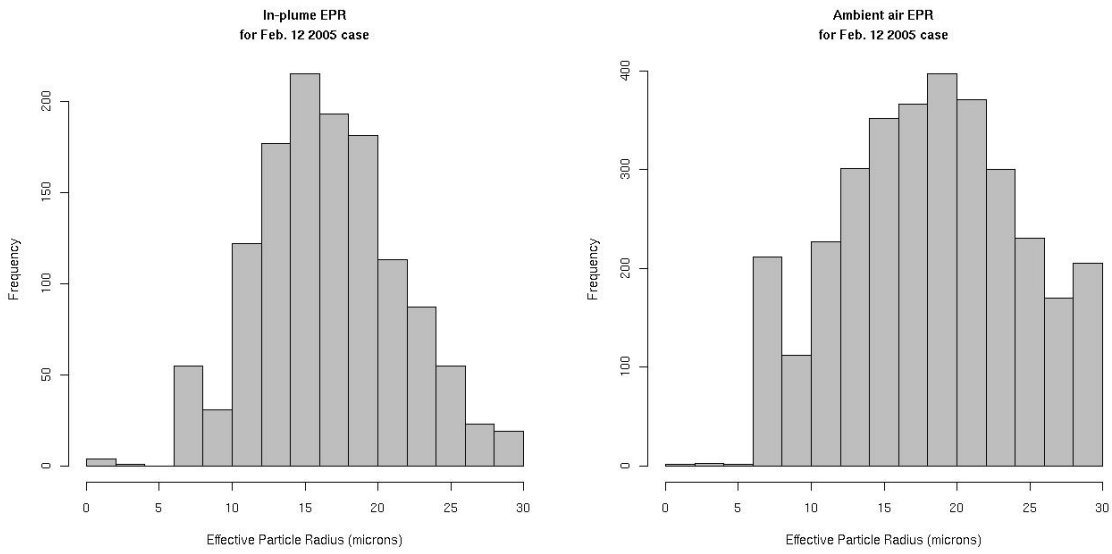

Figure 5.3: Frequency distribution of MODIS EPR data for the February 12 MODIS pass for the in-plume region (left) and the ambient air region (right).

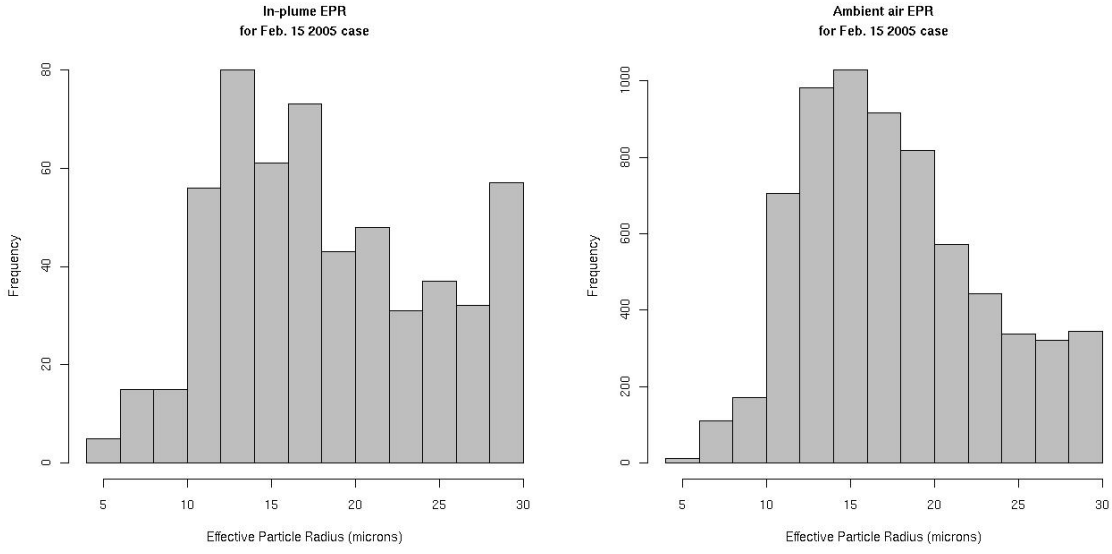

Figure 5.4: Frequency distribution of MODIS EPR data for the February 15 MODIS pass for the in-plume region (left) and the ambient air region (right).

A small number of valid pixels were available for analysis on February 19 compared to the other cases (Figure 5.5). This resulted from the large amount of ice phase pixels present in the study region for this case. The few valid pixels returned EPR values that were mainly above 20 microns. The ambient air region pixels increase in number as the EPR increases to 30 microns. Since widespread glaciation has been established in this case, contamination of the data by ice particles is assured.

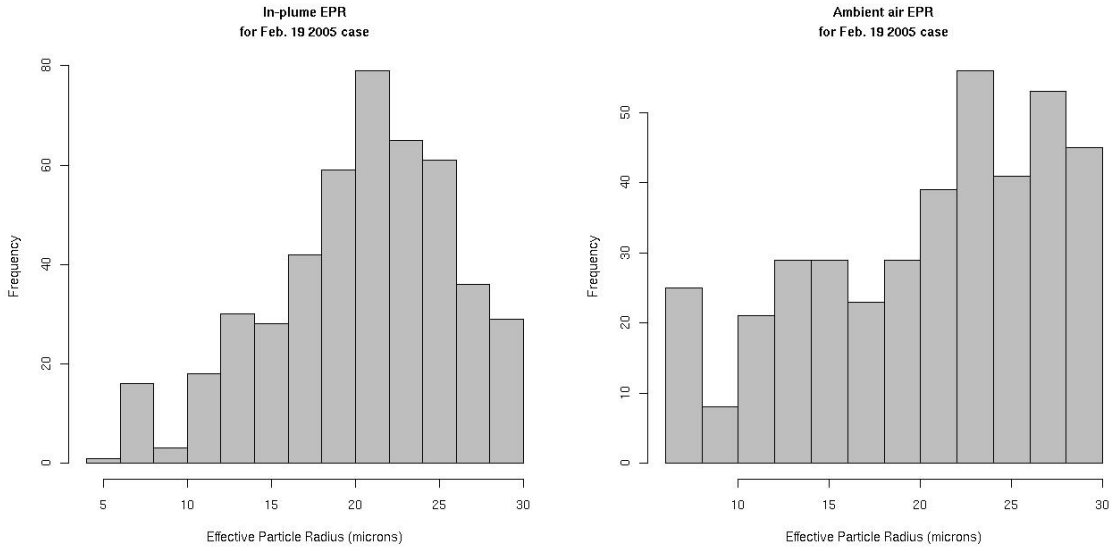

Figure 5.5: Frequency distribution of MODIS EPR data for the February 19 MODIS pass for the in-plume region (left) and the ambient air region (right).

Figure 5.6 compares the frequency distribution of EPR values in-plume and out for February 22. These distributions do not exhibit a clear peak. Both include a rise in the under 12 micron EPR size range, though this rise is much more pronounced in the ambient air figure, and both increase toward the 30 micron cut-off. The February 22 ambient air distribution was the only one that contained a significant portion of EPR

values below 10 microns. The relationship between EPR at cloud top and in lower levels of the cloud for these storms is unclear and will be discussed shortly. Both plots show a large frequency of EPR data above 20 microns, especially the in-plume plot.

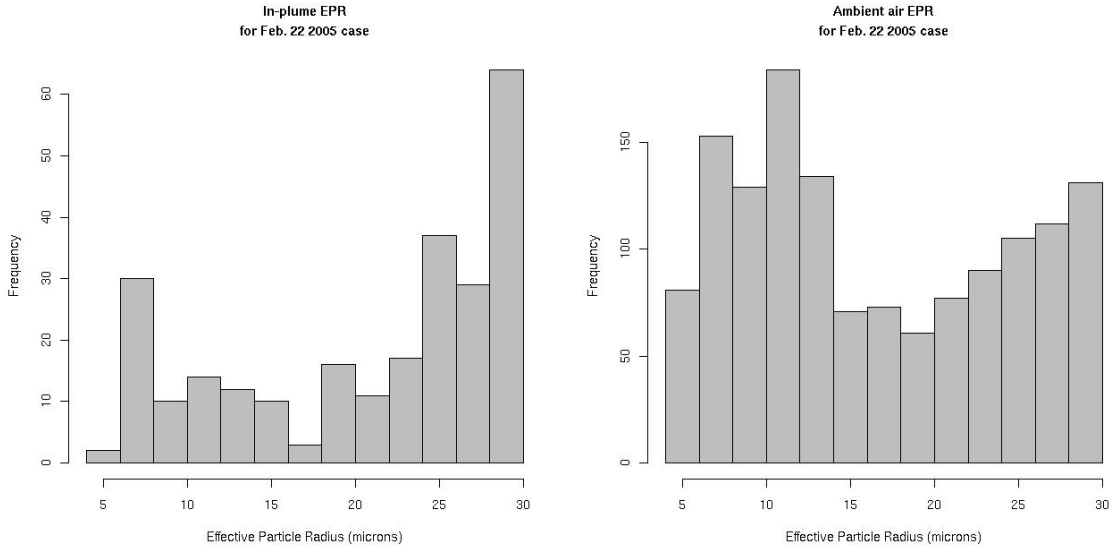

Figure 5.6: Frequency distribution of MODIS EPR data for the February 22 MODIS pass for the in-plume region (left) and the ambient air region (right).

Figure 5.7 investigates the relationship between EPR and COT for all four cases. As reported by Harshvardhan et al. (2002), several observational studies have found that droplet size tends to increase with increasing COT. An in depth modeling investigation by Lohmann et al. (2000) verified these results for optically thin marine clouds (COT < 15). This trend can be seen faintly in a few of the scatterplots in Figure 5.7, most notably the February 12 in-plume plot. High numbers of EPR estimates in the 20-30 micron range at low COT values, seen here for all plots, were not observed in Harshvardhan et

al.'s (2002) marine environment study. Probably these high EPR/low COT pixels are evidence of ice contamination.

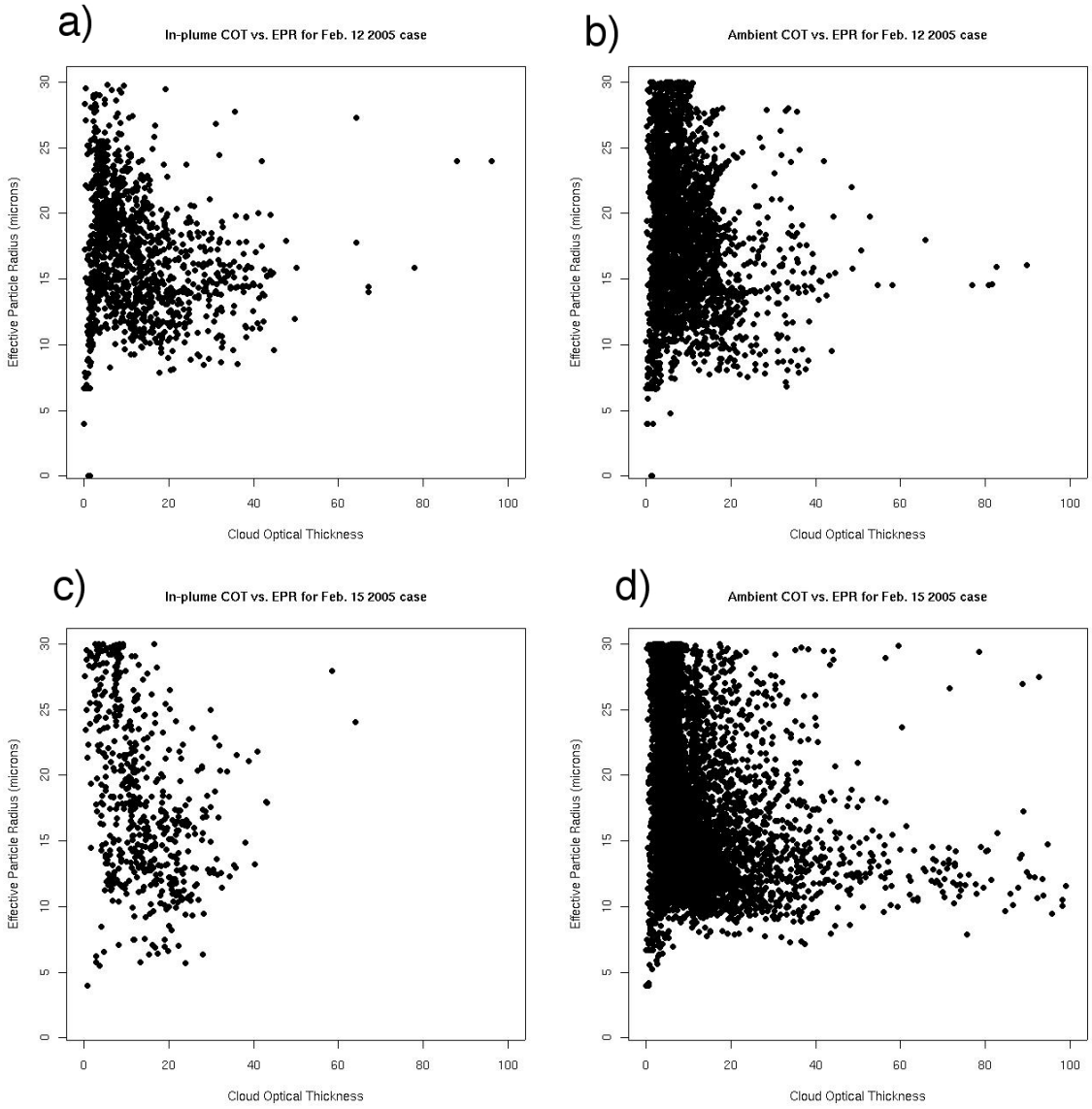

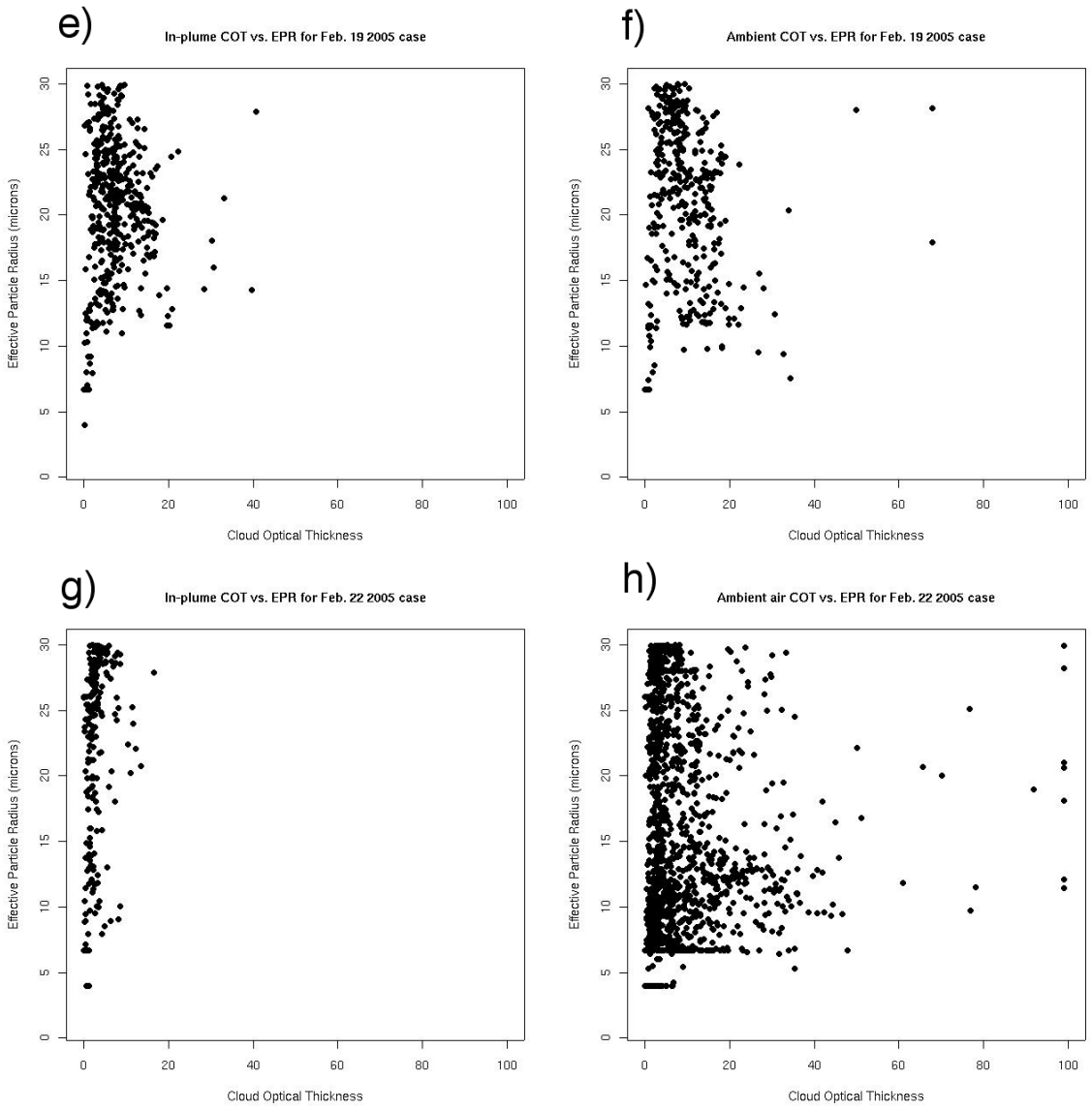

Figure 5.7: Plots of MODIS-derived cloud optical thickness vs. effective particle radius for a) Feb. 12 in-plume, b) Feb. 12 ambient air, c) Feb. 15 in-plume, d) Feb. 15 ambient air, e) Feb. 19 in-plume, f) Feb. 19 ambient air, g) Feb. 22 in-plume, and h) Feb. 22 ambient air.

The in-plume plots for February 15 and 22 show relatively low COT values compared to the ambient air plots for the same dates. The February 12 and 19 cases show similar COT estimates. Otherwise, similar information is given here as was given in the EPR histograms.

Whereas COT depends on the vertical integrals of WP and EPR, WP is directly related to the CDNC and mean volume radius of the droplet spectrum (Brenguier et al., 2000).

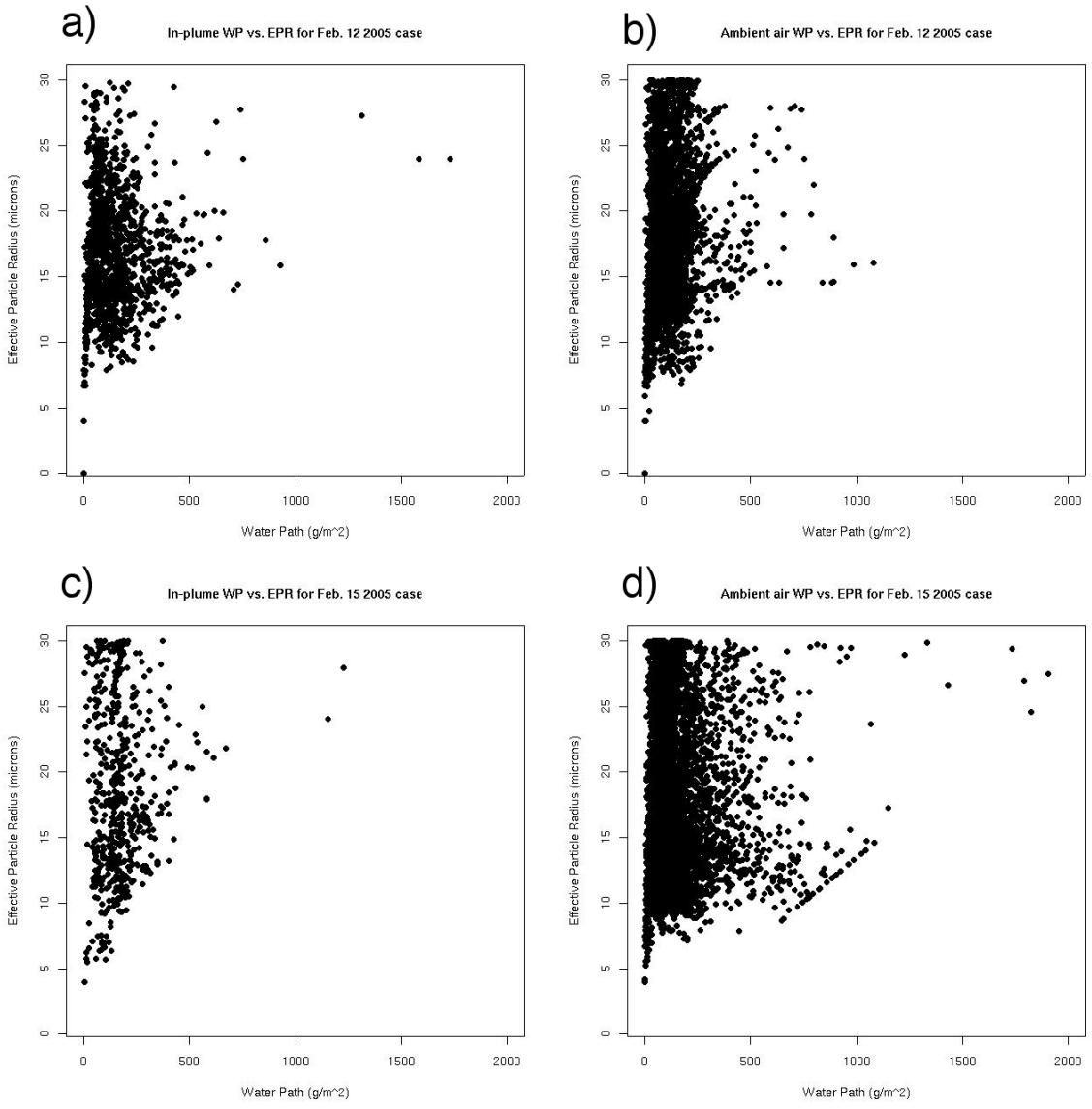

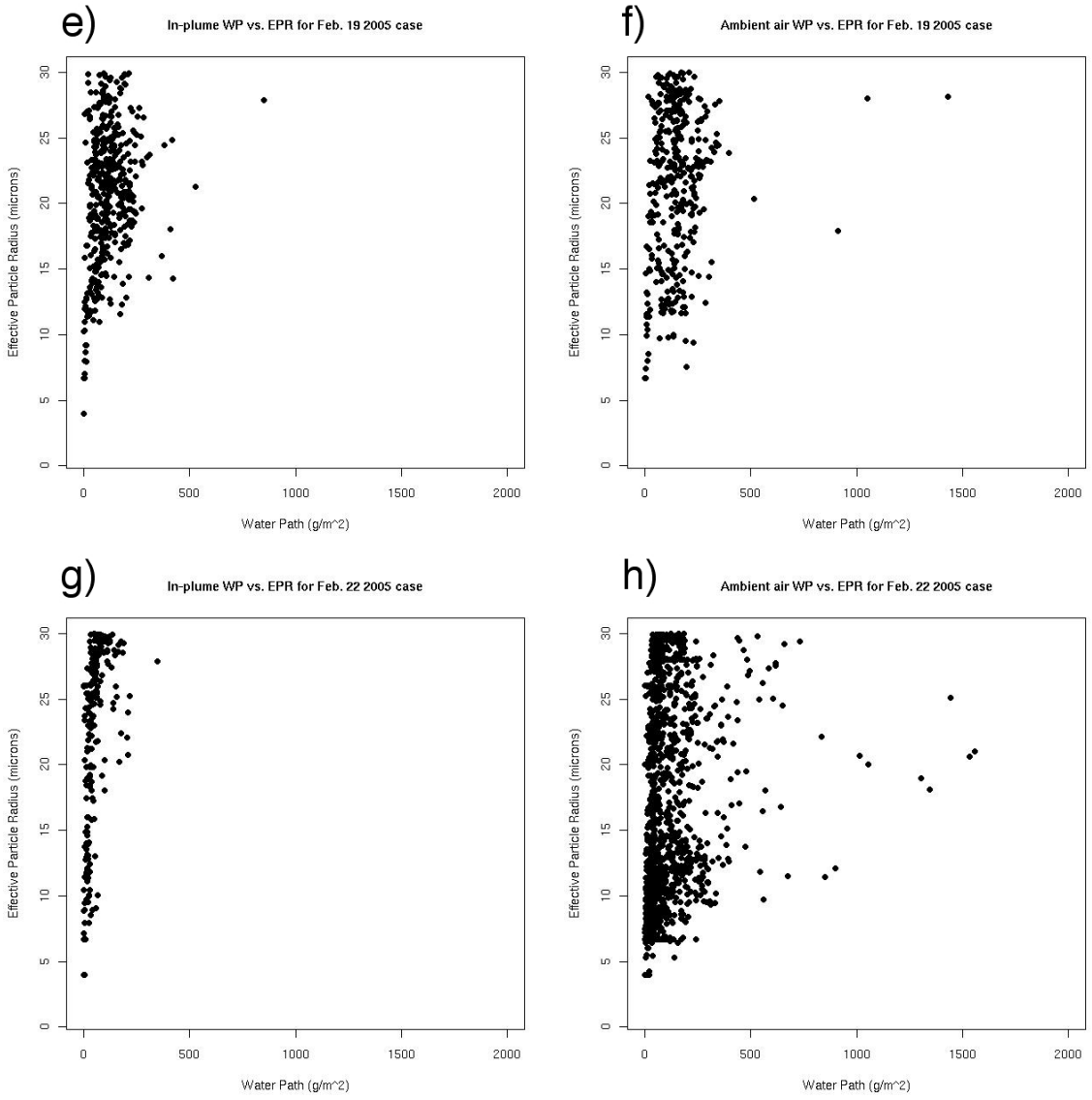

Figure 5.8: Plots of MODIS-derived water path vs. effective particle radius for a) Feb. 12 in-plume, b) Feb. 12 ambient air, c) Feb. 15 in-plume, d) Feb. 15 ambient air, e) Feb. 19 in-plume, f) Feb. 19 ambient air, g) Feb. 22 in-plume, and h) Feb. 22 ambient air.

Therefore, comparisons of EPR estimates for clouds with similar WP values are useful because information about the CDNC can be extracted. Plots of WP vs. EPR are given in Figure 5.8 for all four case studies. EPR increased with increasing WP for low EPR values in most cases. Generally, both in-plume and ambient air regions exhibited similar WP values, with the exception of the February 22 case. Although the February 22 in-plume plot included only a small number of pixels with low EPR for comparison to the ambient air plot.

Possible ice contamination again makes itself known with high EPR, low WP pixels. This recurring theme is a major problem in conducting this analysis. It is impossible to be certain that liquid water data are untainted by ice particles even when the MODIS cloud phase estimates a pixel to be liquid phase.

5.1.3 Vertical extent of emissions

Another issue with the use of MODIS reflectance measurement products is the cloudtop location of such measurements. In a modeling study, Brenguier et al. (2000) put forward a relationship between the cloud top EPR and particle size in the lower cloud levels but suggested it was not a constant relationship. The satellite's view of EPR at cloudtop may not be representative of particle sizes in the mid and lower levels of the cloud. This is especially true in clouds of an orographic nature. As described by Borys et al. (2000), vertical mixing is often limited in orographic clouds, limiting particle movement to

mainly horizontal trajectories through the cloud. This is a large problem for a satellite analysis of these clouds.

MODIS retrievals estimated cloud top temperatures around 240 K for the February 12 and 19 cases. The low temperature at cloud top indicates high cloud heights, although COT estimates for these clouds were not comparatively high next to the two remaining cases. The cloud top temperature estimates for the 15th and 22nd in the Park Range region varied between about 260-270K with lower values to the north and east on the 22nd.

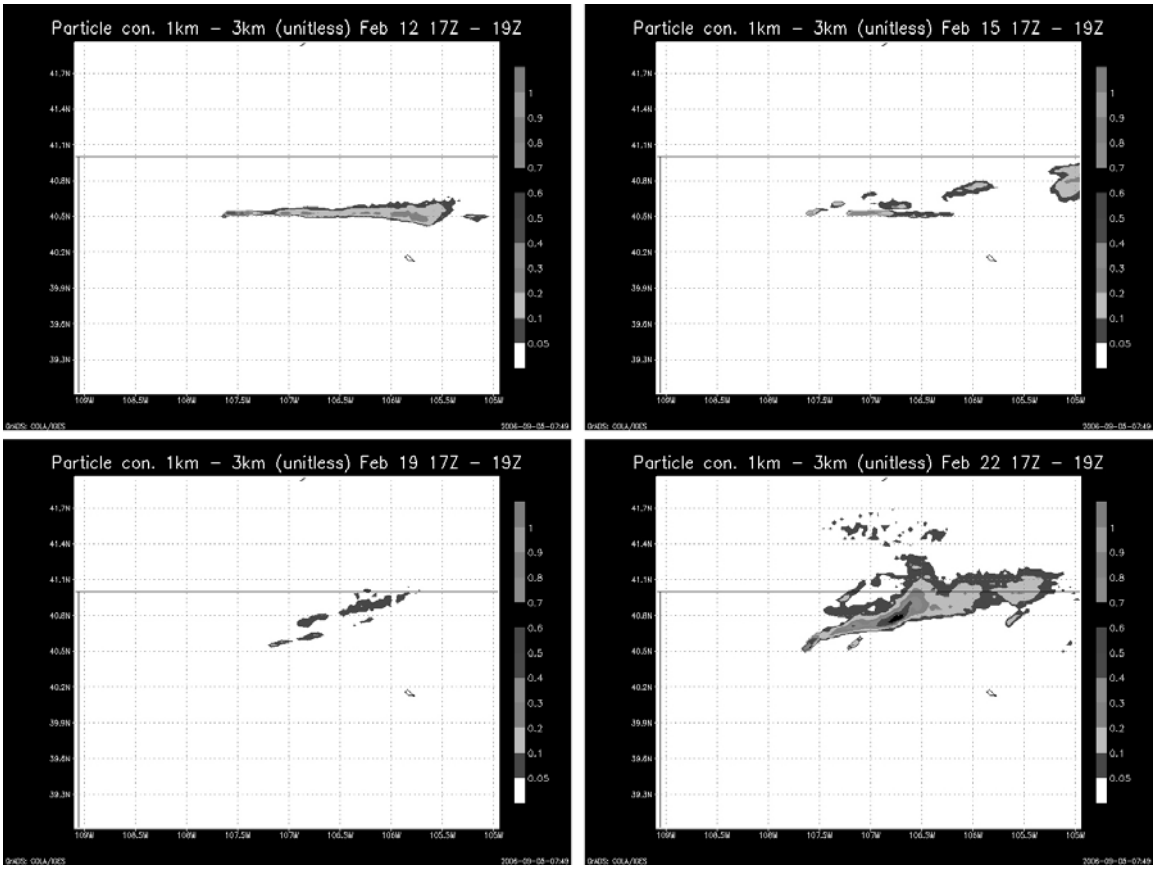

Figure 5.9: LPD model output particle concentration of the 1-3km layer for 17:00Z to 19:00Z on February 12 (top left), February 15 (top right), February 19 (bottom left), February 22 (bottom right).

This begs the question, did the emissions from the Craig and Hayden power plants extend high enough to influence cloud microphysics where MODIS could observe their impact? This is especially important for the two cases with relatively high cloud tops. Figures 5.9 and 5.10 examine this question by showing particle concentrations in different vertical layers of the atmosphere for all four cases. The layer heights represent height above ground level, which varies with the topography.

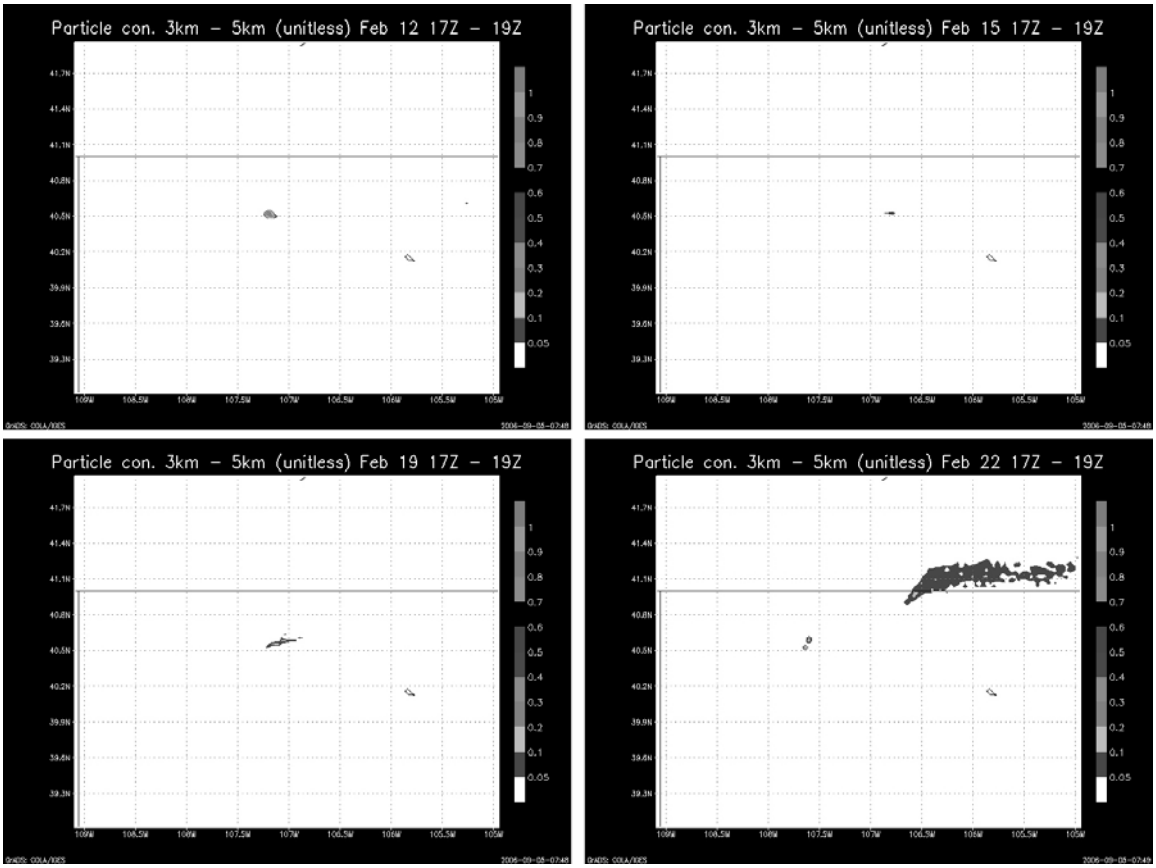

Figure 5.10: LPD model output particle concentration of the 3-5km layer for 17:00Z to 19:00Z on February 12 (top left), February 15 (top right), February 19 (bottom left), February 22 (bottom right).

In accordance with the Borys et al. (2000) orographic cloud model, the particles remain in the low to mid levels of the atmosphere. Almost no particles were predicted to rise above 3 km in these cases. According to Rauber and Grant (1986), a cloud top temperature of 243K in the Park Range typically corresponds to a cloud top height near 7km above sea level, or approximately 4km above even the high terrain of the Park Range. Thus the emission plumes may not have reached the cloud top observing level of the MODIS instrument in the February 12 and 19 cases.

5.2 Snowfall rate

The satellite inspection revealed interesting information about the four storm cases, although no hard evidence of an aerosol effect. Possible aerosol effects on cloud processes will be viewed from a different perspective in this section using the SNOTEL and SPL snowfall measurements. Evidence of decreased precipitation rate in a high sulfate environment has already been measured at SPL (Borys et al., 2003). In that case snowfall rate was determined using measurements taken about every 5 minutes. Also, they were concerned with just one sampling location, meaning the measurement period could be limited to the time when snow was falling at that location.

The current study evaluates snapshots in time to allow for regional analysis including many sampling sites. Therefore the time period used to calculate precipitation rate should be universal across all sampling sites whether snow was continuously falling during that period or not. If the time period chosen covers many hours, observations that

occurred in different plume and cloud environments may be included in the precipitation rate calculation. On the other hand, the sampling period must be long enough to span the time when precipitation fell at all sites. Small differences in precipitation timing from one SNOTEL site to the next could lead to excluded data if only one data point is used. With the SNOTEL observations reported every hour in most cases, this means the sampling period must be at least 2 hours long.

Most of the SNOTEL sites report SWE measurements every hour. The sites at Buffalo Park (913) and Lynx Pass (607) only reported SWE in 2-hour intervals and at Lost Dog (940), Columbine (408) and Crosho (426), data were only available in 3-hour intervals. To be certain the measurements were collected from similar environmental conditions

SNOTEL site	ID#		Feb. 12		Feb. 15		Feb. 19		Feb. 22
Elk River	467		17Z-20Z		17Z-20Z		17Z-20Z		16Z-19Z
Lost Dog	940		16Z-19Z		16Z-19Z		16Z-19Z		16Z-19Z
Zirkel	1033		17Z-20Z		17Z-20Z		17Z-20Z		16Z-19Z
Dry Lake	457		17Z-20Z		17Z-20Z		17Z-20Z		16Z-19Z
Tower	825		17Z-20Z		17Z-20Z		17Z-20Z		16Z-19Z
Columbine	408		16Z-19Z		16Z-19Z		16Z-19Z		16Z-19Z
Rabbit Ears	709		17Z-20Z		17Z-20Z		17Z-20Z		16Z-19Z
Arapaho Ridge	1030		17Z-20Z		17Z-20Z		17Z-20Z		16Z-19Z
Buffalo Park	913		16Z-20Z		16Z-20Z		16Z-20Z		16Z-20Z
Crosho	426		16Z-19Z		16Z-19Z		16Z-19Z		16Z-19Z
Lynx Pass	607		16Z-20Z		16Z-20Z		16Z-20Z		16Z-20Z
Bear River	1061		17Z-20Z		17Z-20Z		17Z-20Z		16Z-19Z
Ripple Creek	717		17Z-20Z		17Z-20Z		17Z-20Z		16Z-19Z
Trapper Lake	827		17Z-20Z		17Z-20Z		17Z-20Z		16Z-19Z
Burro Mountain	378		17Z-20Z		17Z-20Z		17Z-20Z		16Z-19Z
Bison Lake	345		17Z-20Z		17Z-20Z		17Z-20Z		16Z-19Z

Table 5.2: The snowfall sampling period for all SNOTEL sites for all cases.

from all sites, a sampling period of 3 hours was used to determine precipitation rate. In the case of Buffalo Park and Lynx Pass, a 4-hour sampling period was used to accommodate the 2-hour measurements. The sampling periods were centered around the MODIS overpass time and the time of the power plant plume analysis (17Z-19Z). Table 5.2 lists the time periods used for each station and case to calculate the precipitation rate.

The accumulation of SWE was used as a measure of precipitation rate for these cases. SWE was also used by Borys et al. (2003) to assess precipitation rate and Saleeby and Cotton (2005) as a measure of total precipitation in the Park Range. The average

SNOTEL site	#		Feb. 12	Feb. 15	Feb. 19	Feb. 22
			ave.	ave.	ave.	ave.
Elk River	467		0.17	0.85	0.25	0.85
Lost Dog	940		0.17	0.85	0.25	0.00
Zirkel	1033		0.85	0.59	0.85	1.19
Dry Lake	457		0.59	1.69	1.19	1.02
Tower	825		0.85	1.44	0.59	0.59
Columbine	408		2.03	1.44	2.29	1.86
Rabbit Ears	709		0.17	1.02	0.25	0.25
Arapaho Ridge	1030		0.59	0.25	0.59	0.68
Buffalo Park	913		0.17	0.17	0.42	0.44
Crosho	426		1.02	1.86	1.10	1.44
Lynx Pass	607		0.68	0.59	0.34	1.84
Bear River	1061		0.85	0.42	0.42	0.85
Ripple Creek	717		0.42	1.02	0.42	0.42
Trapper Lake	827		0.59	1.86	0.59	1.27
Burro Mountain	378		0.85	0.68	0.42	0.59
Bison Lake	345		0.42	7.20	0.42	0.25
Average			0.65	1.37	0.65	0.85
In-Plume Average			0.61	1.57	0.45	0.68
Ambient Average			0.66	1.34	0.70	0.89

Table 5.3: Average snowfall rate at the SNOTEL sites for the sampling periods listed in Table 5.2. Sites that were located in-plume are shaded in grey. The average of all sites, and average for in-plume and ambient air regions are listed at the bottom.

precipitation rate for all SNOTEL sites and all four storm cases are given in Table 5.3. The sites that lie under the model-forecasted power plant plume are shaded grey.

Only the northern-most SNOTEL sites were located in-plume as follows from the generally eastward and northward dispersion of particles in all four cases. This is unfortunate as it leads to miniscule in-plume sample sizes, severely limiting statistical analysis available for comparing in-plume and ambient air data groups. Also, it eliminates the opportunity to compare the snowfall at the northern sites when they lie under the plume to when they are located in the ambient environment.

The mean precipitation rate was lower for the in-plume sites than the ambient air sites for the February 12, 19 and 22 storms. The February 15 in-plume sites measured a considerably higher precipitation rate than sites out of the plume, though only 2 SNOTEL sites were used to determine the in-plume average rate. Table 5.4 shows the SNOTEL precipitation rate data ranked by the measured precipitation rate in ascending order. In-plume locations can be identified by grey shading. Where several stations reported the same precipitation rates, the stations were ordered by ascending station number. The ranked data does not suggest a relationship between precipitation rate and location within the model-predicted power plant plume. While the three cases with lower in-plume precipitation rate contained a site that matched the lowest observed rate for that case, they also included sites with relatively high rates.

Feb. 12 ave.	**Feb. 15** ave.	**Feb. 19** ave.	**Feb. 22** ave.
0.17	0.17	0.25	0.00
0.17	0.25	0.25	0.25
0.17	0.42	0.25	0.25
0.17	0.59	0.34	0.42
0.42	0.59	0.42	0.44
0.42	0.68	0.42	0.59
0.59	0.85	0.42	0.59
0.59	0.85	0.42	0.68
0.59	1.02	0.42	0.85
0.68	1.02	0.59	0.85
0.85	1.44	0.59	1.02
0.85	1.44	0.59	1.19
0.85	1.69	0.85	1.27
0.85	1.86	1.10	1.44
1.02	1.86	1.19	1.84
2.03	7.20	2.29	1.86

Table 5.4: The same data as in Table 5.3. Here they are ranked in order of snowfall rate magnitude for each individual storm case. The in-plume sites can be identified by the grey shading.

SPL was located in-plume for the February 12, 15 and 19 cases. During the February 12 and 19 sampling periods, SPL recorded no precipitation. On February 15, a rate of 1.27 mm/hr was measured and on February 22, 0.76 mm/hr of SWE fell. If these data were included with the SNOTEL data, they would in all cases bring down the average precipitation rate of the group it is located in. The SPL data supports possible suppression of precipitation in the February 12 and 19 in-plume cases, but not for February 15.

5.3 Discussion

The results presented above do not suggest a connection between the Craig and Hayden power plant emissions and suppression of snowfall due to decreased riming efficiency. There may be several reasons for this outcome. The influence of synoptic weather patterns and small-scale cloud processes will be discussed as well as issues with the methods used to investigate the aerosol effects. This discussion will be carried out considering each storm separately since each case exhibited a unique environment.

5.3.1 February 12 case

The February 12 storm had a low CTT and was optically thick compared to the similar CTT February 19 case as determined by MODIS measurements. Unfortunately, the large amounts of ice particles indicated by the MODIS cloud phase product make inferences about the mid and lower cloud layers nearly impossible. Rauber and Grant (1986) classify 30-40% of the storms they observed in northwestern Colorado as deep stratiform systems with CTT's similar to those observed for the February 12 case. However, their illustration of this storm type included widespread heavy precipitation in most cases. On February 12, 2005 the average precipitation rate for all SNOTEL sites was less than 1 mm/hr.

If this case does fall into the deep stratiform storm classification of Rauber and Grant (1986), the entire cloud layer likely consisted of ice particles. This could reduce the

importance of riming in this event and diminish the impact of high aerosol concentrations on precipitation rate. Aside from this deep stratiform storm model, Hill (1980) found that supercooled liquid water concentration near the barrier crest in orographic clouds decreases with decreasing CTT. It was also found that the amount of supercooled water increased with increasing cross-barrier wind speed when this wind speed was over 10 m/s. Observed average wind speed at SPL, which is situated on the Park Range barrier crest, was about 9 m/s for the period of 16Z-19Z on February 12.

5.3.2 February 15 case

This case looked to be the best candidate to demonstrate any impact of the power plant plumes on local storms. The forecasted plumes for both Craig and Hayden were concentrated over the Park Range and MODIS products indicated shallow, mainly liquid-phase clouds. Half of the precipitation observation sites reported rates of SWE accumulation over 1mm/hr, including those sites within the forecasted plume. Satellite EPR retrievals showed similar EPR values for both in-plume and ambient air regions.

The February 15 storm exhibited the greatest MODIS-derived WP values of all four cases, and it also contained far more valid data pixels. The abundant data in this case may be due to high CTT's that inhibited ice particle formation. CTT's near 260K for much of the study region in this case suggest a thin stratiform layer storm, a form also observed by Rauber and Grant (1986) in approximately 30-40% of storm cases in the Park Range. Storms of this type studied by Rauber and Grant (1986) had the potential to

produce significant amounts of supercooled liquid water, though the observed amounts varied. The large WP values found on February 15 are consistent with the Rauber and Grant (1986) shallow stratiform model. Relatively large amounts of supercooled liquid water could theoretically lead to higher precipitation rates through an increase in riming efficiency assuming a constant droplet size spectrum.

In a modeling study of Arctic clouds, Lohmann (2003) found that riming and snowfall rates in polluted clouds were initially increased over that of cleaner clouds. However, the total precipitation produced by the polluted cloud was less than that of the clean cloud (Lohmann, 2003). Since the sampling period used for the February 15 case fell near the beginning of the snowfall event at most of the SNOTEL sites, it is worth looking at the total accumulated precipitation for the event. Fortunately, the emission plume location

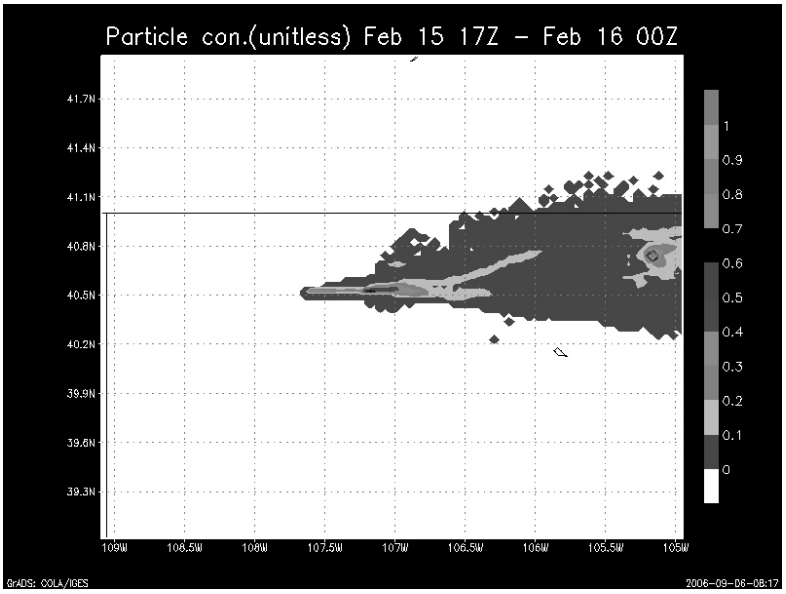

Figure 5.11: Particle concentration for the 0-10km layer averaged over the time period between 17:00Z February 15 and 00:00Z February 16.

did not vary much through 00:00Z February 16 (Figure 5.11). After 00:00Z most sites stopped reporting increases in SWE. Table 5.6 shows the total precipitation for 16Z Feb 15 to 00Z Feb 16. The two in-plume sites in this case reported high amounts of accumulated SWE compared to the majority of other sites. If the power plant emissions reduced droplet size in this case, it likely was not reduced enough to shut down heavy riming.

SNOTEL site	**#**		**Feb. 15** Total precip (mm)
Elk River	467		5.08
Lost Dog	940		3.05
Zirkel	1033		3.05
Dry Lake	457		7.62
Tower	825		7.37
Columbine	408		4.32
Rabbit Ears	709		4.32
Arapaho Ridge	1030		2.54
Buffalo Park	913		1.78
Crosho	426		9.91
Lynx Pass	607		4.06
Bear River	1061		4.32
Ripple Creek	717		5.08
Trapper Lake	827		5.84
Burro Mountain	378		3.81
Bison Lake	345		27.94

Table 5.5: Total precipitation for the period 16:00Z February 15 to 00:00Z February 16 at all SNOTEL sites. In-plume sites are shaded grey.

5.3.3 February 19 case

As with the February 12 case, widespread glaciation limited the amount of information MODIS could provide for the February 19 storm. Though a similarly low CTT in this case suggests that available supercooled water may have been limited in the cloud lower levels (Hill, 1980). Incidentally, the average wind speed at SPL for the February 19 sampling period was about 11 m/s.

Precipitation rates measured at the SNOTEL sites were remarkably similar to the measurements from the February 12 case (see Table 5.3), but the predicted plume location contained different SNOTEL sites in each case. Two sites that were in-plume on the 12th were in the ambient air region on the 19th. The precipitation rate at Dry Lake, in-plume on the 12th, was twice as high on the 19th when it was in the ambient air region. On the other hand, the Tower site precipitation rate decreased from 0.85 mm/hr to 0.59 mm/hr as it went from in-plume on the 12th to ambient air on the 19th. The one site that was in-plume on the 19th and not on the 12th reported similar precipitation rates on both dates.

Again, no connection between the forecasted plume location and precipitation rate on the ground is apparent. It's possible, as with the February 12 case, that liquid water was not available in large quantities for this storm.

5.3.4 February 22 case

The MODIS-derived EPR field for the February 22 storm shows a cloud-top environment containing small droplets in areas where liquid water particles are indicated. The CTT product reveals that these liquid cloudwater areas are co-located with areas of relatively high CTT and presumably lower cloud heights (Figure 5.12). The CTT image suggests this storm may have included a shallow stratiform layer near the surface overlayed by a patchy layer of high clouds that mainly consisted of ice.

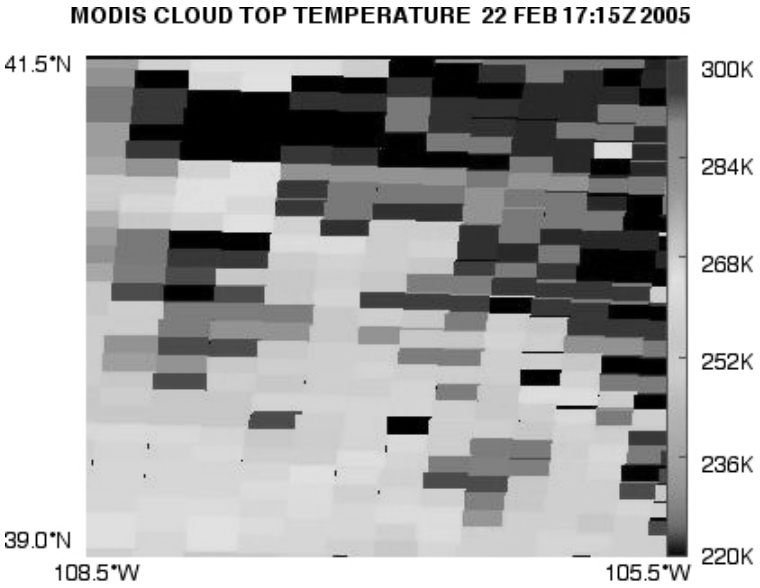

Figure 5.12: MODIS cloud top temperature product for the study region for the February 22 overpass.

The three SNOTEL sites with the highest precipitation rate for this case were located in the southern Park Range and northern Flattops in a region where MODIS indicated low EPR values at cloud top. One of the three stations with the lowest precipitation rate (Rabbit Ears) was also located here. This region provided the sub-10 micron EPR values

that were only seen in a large proportion for the February 22 case. The power plant emissions were located well to the north of the pocket of low EPR values at this time.

Behind the physical reasoning lies the possibility that the methods employed in this study were not sufficient to truly observe small effects of CCN on precipitation. Since aerosol concentrations were not measured for the study region but estimated from dispersion model output and past work, the true CCN concentration field cannot be substantiated. Therefore CCN effects, or the lack thereof, can be inferred but not confirmed for these cases. In addition, the abundance of ice particles at cloud top severely limited analysis of liquid water processes in the February 12 and 19 cases. While more liquid water was present in the other two cases, the orographic nature of these storms is such that the satellite view may not contain a lot of information about the lower levels of clouds. The conclusions that can be reached by these methods are outlined in the next section, along with suggestions for future work.

Chapter 6 – Conclusions and Suggestions for Future Research

6.1 Summary

A dispersion model was employed to simulate particle emission from the Craig and Hayden power plants in northwestern Colorado. The model output was used to determine regions affected by the power plant plumes and regions outside their influence for four winter storm cases in February 2005. The environment inside these regions was investigated using MODIS data products. The EPR was of particular interest and was compared to the COT and WP for in-plume and ambient air regions. No significant aerosol effect was discernable using the MODIS data.

To explore possible effects on surface precipitation rate from the power plant emissions, SWE accumulation data from SNOTEL sites and SPL were examined. The average in-plume precipitation rate for three of the storms was less than that in the ambient air, but the sample size of in-plume sites was small and they were in the northern part of the study region for all cases. In addition, ranking the measurements revealed that there was no observable connection between precipitation rate and in-plume location in these cases, although more robust statistics are needed to discern any trends in snowfall rate.

6.2 Conclusions

The purpose of this project was to investigate the effects of power plant emissions on local winter storm cloud processes and precipitation. The results of the study were mostly inconclusive. Of the four cases scrutinized, the February 15 case provided conditions most favorable for satellite observation of liquid cloud properties (i.e. relatively warm cloud top, mainly liquid phase particles at cloud top according to the MODIS cloud-phase product). The non-diffuse plume forecast output by the LPD model gave a clear indication of where high sulfate and nitrate concentrations could be expected in this case. After analysis of the MODIS data products and surface precipitation data, no difference between the in-plume and ambient air regions could be discerned.

While the miniscule sample of surface precipitation data located in-plume limited the legitimacy of analysis for this case, it's possible the addition of atmospheric particles from the power plants was not substantial enough to cause a visible aerosol effect. Past studies of isolated coal power plant plumes have found that in-plume CCN levels are typically many times higher than that of the ambient air even over 100km from the source (Hobbs et al., 1980; Mamane and Pueschel, 1980, etc.). But CCN concentrations were not directly measured in this study, leaving the possibility that the defined in-plume region was not significantly CCN-rich compared to the ambient environment. CN measurements from SPL might help to confirm or deny the plume location.

A major conclusion of this paper is that visible and infrared satellite retrievals may simply be inappropriate for a study of this kind. Previous work has shown success using similar methods but with relatively warm clouds (Rosenfeld, 1999; Rosenfeld, 2000; Harshvardhan et al., 2002) or on a global scale (Breon et al., 2002). The presence of ice in many northwestern Colorado winter storms and interference of the mountainous and snow-covered underlying surface reduced the usefulness of the retrieved data. In addition, only weak vertical mixing in most orographic clouds may prevent the satellite from viewing a cloud environment that is representative of the lower cloud levels. This would limit satellites' ability to observe in-cloud processes even for liquid water phase orographic clouds.

Variations in measured precipitation from storm to storm for the SNOTEL sites suggest other forces besides Criag and Hayden emissions are driving the snowfall rate. Other large regional sources of aerosol may have unexpectedly contributed to CCN in the studied winter storms. If contamination by other sources were significant, the designations of in-plume and ambient air regions would have been inaccurate. Also, it's likely that the large-scale weather forcing or variations in small-scale flow due to topography had a more substantial impact on snowfall rate on a case-by-case basis than local aerosol sources.

As stated by Hindman et al. (1994), a relationship must be established between clean clouds and lack of anthropogenic CCN and polluted clouds and a source of anthropogenic CCN before conclusions can be made about the magnitude of the effects of

anthropogenic CCN on cloud droplet spectra at SPL. While recent studies by Borys et al (2000,2003) have provided excellent data and deductions on this topic, and the current study gives a different view, more work could be done. Possible directions for this work are submitted for consideration in the next section.

6.3 Suggestions for future research

Despite the results of this study, the Park Range area is an excellent arena for study of orographic winter storms and aerosol effects on microphysical processes. As a study region it was improved in March 2006 with the installation of a CCN counter at SPL. This will provide semi-continuous CCN spectrum data from the free troposphere. Future studies of this kind could use the CCN data from SPL for verification of model output and, in conjunction with FSSP droplet spectrum measurements, monitor the behavior of the CCN spectrum before, after and during winter storm events.

Jirak and Cotton (2006) used over 50 years of precipitation data to investigate precipitation trends in upslope precipitation along the Colorado Front Range. They found for upslope storm events a decreasing trend in precipitation downwind of expanding metropolitan areas that was attributed to increased city aerosol production. Comparable results were found in mountains in Israel and California by Givati and Rosenfeld (2004). A similar method was applied to the Hayden-Steamboat Springs corridor and many other sites across the western United States as reported by Rosenfeld and Givati (2006), although wind direction during precipitation events was not considered in that study.

Assuming the Craig and Hayden towns and power plants are the major local aerosol sources upwind of Steamboat Springs, the mean wind direction during winter storms in this region could greatly influence the aerosol concentration in the atmosphere above Steamboat Springs. This is suggested by the results of the dispersion model described in Chapter 4. Jirak and Cotton (2006) included wind criteria in their analysis of upslope storms, a method that could be applied to northwestern Colorado. According to Bluemenstein et al. (1987), the wind speed may have as drastic an effect on orographic precipitation as the wind direction. Unfortunately, the high particle source height of the power plant plumes could render surface wind observations, such as those used by Jirak and Cotton (2006), inadequate for this case.

Finally, to truly understand the potential effects of the Craig and Hayden plants on atmospheric CCN and cloud processes in the Park Range, regional *in situ* observations are needed. While SPL provides valuable data, essential for a study of this kind, aircraft observations, such as those used by Rauber et al. (1986) and Mamane and Pueschel (1980), would expand this data collection for the region. With aircraft, the chemistry and extent of plume dispersion from Craig and Hayden could be determined and the impact of these sources on the ambient aerosol concentration learned. As in Rauber et al. (1986), detailed information about the cloud microphysics could be obtained. The scale of such a project would be massive, but could more ably confirm or deny the effect of local sulfate and nitrate sources on winter clouds in the Park Range than modeling or remote sensing techniques.

REFERENCE LIST

Ackerman, Steven A., Kathleen I. Strabala, W. Paul Menzel, Richard A. Frey, Christopher C. Moeller, and Liam E. Gumley, 1998: Discriminating clear sky from clouds with MODIS. *J. Geophys. Res*., **103**, No. D24, 32,141-32,157.

Bluemenstein, Rochelle R., Robert M. Rauber, Lewis O. Grant, and William G. Finnegan, 1987: Application of ice nucleation kinetics in orographic clouds. *J. Climate Appl. Meteor*., **26**, 1363-1376.

Borys, Randolph D., Douglas H. Lowenthal, Stephen A Cohn, and William O. J. Brown, 2003: Mountaintop and radar measurements of anthropogenic aerosol effects on snow growth and snowfall rate. *Geophys. Res. Letters*, **30**, No. 10, 1538, doi:10.1029/2002GL016855, 2003.

Borys, Randolph D., Douglas H. Lowenthal, and David L. Mitchell, 2000: The relationship among cloud microphysics, chemistry, and precipitation rate in cold mountain clouds. *Atmos. Environ*., **34**, 2593-2602.

Borys, Randolph D., Douglas H. Lowenthal, and Kenneth A. Rahn, 1986: Contributions of smelters and other sources to pollution sulfate at a mountaintop site in northwestern Colorado. Acid Deposition in Colorado – A Potential or Current Problem; Local versus Long-Distance Transport into the State. Colorado State University, Fort Collins, pp. 167-174.

Borys, Randolph D., and Melanie A. Wetzel, 1997: Storm Peak Laboratory: A research, teaching, and service facility for the atmospheric sciences. *Bull. Amer. Meteor. Soc*., **78**, No. 10, 2115-2123.

Boucher, Olivier, and Ulrike Lohmann, 1995: The sulfate-CCN-cloud albedo effect. *Tellus*, **47B**, 281-300.

Brenguier, Jean-Louis, Hanna Pawlowska, Lothar Schuller, Rene Preusker, Jurgen Fischer, and Yves Fouquart, 2000: Radiative properties of boundary layer clouds: Droplet effective radius versus number concentration. *J. Atmos. Sci*., **57**, 803-821.

Breon, Francios-Marie, Didier Tanre, and Sylvia Generoso, 2002: Aerosol effect on cloud droplet size monitored from satellite. *Science*, **295**, 834-838.

Briggs, G. A., 1975: Plume rise predictions. P*roceedings, Lectures on Air Pollution and Environmental Impact Analyses*, D Haugen, Ed., American Meteorological Society, 59-111.

Cantrell, B. K. and K. T. Whitby, 1978: Aerosol size distributions and aerosol volume formation for a coal-fired power plant plume. *Atmos. Environ*., **12**, 323-333.

Colle, Brian A., 2004: Sensitivity of orographic precipitation to changing ambient conditions and terrain geometries: An idealized modeling perspective. *J. Atmos. Sci*., **61**, 588-606.

Cotton, W. R., R. A. Pielke Sr., R. L. Walko, G. E. Liston, C. J. Trembeck, H. Jiang, R. L. McAnelly, J. Y. Harrington, M. E. Nichols, G. G. Carrio, and J. P. McFadden, 2003: RAMS 2001: Current status and future directions. *Meteor. Atmos. Physics*, **82**, 5-29.

DeMott, P.J., D.J. Cziczo, A. J. Prenni, D. M. Murphy, S. M. Kreidenweis, D. S. Thomson, R. Borys, and D.C. Rogers, 2003: Measurements of the concentration and composition of nuclei for cirrus formation. *Proceedings of the Nat. Academy of Sciences*, **100**, No. 25, 14655-14660.

Givati, Amir, and Daniel Rosenfeld, 2004: Quantifying precipitation suppression due to air pollution. *J. Appl. Meteor*., **43**, 1038-1056.

Gunn, Ross, and B. B. Phillips, 1957: An experimental investigation of the effect of air pollution on the initiation of rain. *J. Meteor*., **14**, 272-280.

Hallberg, A., J. A. Ogren, K. J. Noone, K. Okada, J Heintzenberg, and I. B. Svenningsson, 1994: The influence of aerosol particle composition on cloud droplet formation. *J. Atmos. Chem*., **19**, 153-171.

Hanna, Steven R., 1972: Rise and condensation of large cooling tower plumes. *J. Appl. Meteor*., **11**, 793-780.

Harrington, J. Y., 1997: The effects fo radiative and microphysical processes on simulated warm and transition season Arctic stratus. Ph. D. dissertation, Colorado State University, 289 pp.

Harshvardhan, S. E. Schwartz, C. M. Benkovitz, and G. Guo, 2002: Aerosol influence on cloud microphysics examined by satellite measurements and chemical transport modeling. *J. Atmos. Sci.,* **59**, 714-725.

Haywood, James, and Olivier Boucher, 2000: Estimates of the direct and indirect radiative forcing due to tropospheric aerosols: A review. *Rev. Geophys.,* **38**, 513-543.

Hill, E. Geoffrey, 1980: Seeding-opportunity recognition in winter orographic clouds. *J. Appl. Meteor*., **19**, 1371-1381.

Hindman, E.E., E. J. Carter, R. D. Borys, and D. L. Mitchell, 1992: Collecting supercooled cloud droplets as a function of droplet size. *J. Atmos. Oceanic Technol*., **9**, 337-353.

Hindman, Edward E., Mechel A. Campbell, and Randolph D. Borys, 1994: A ten-winter record of cloud-droplet physical and chemical properties at a mountaintop site in Colorado. *J. Appl. Meteor*., **33**, 797-807.

Hobbs, Peter V., Jeffrey L. Stitch, and Lawrence F. Radke, 1980: Cloud-active nuclei from coal-fired electric power plants and their interactions with clouds. *J. Appl. Meteor*., **19**, 439-451.

Hudson, J. G., 1991: Observations of anthropogenic cloud condensations nuclei. *Atmos. Environ.,* **25A**, 2449-2455.

Husar, R. B., D. E. Patterson, J. D. Husar, N. V. Gillani, and W. E. Wilson, Jr., 1978: Sulfur budget of a power plant plume. *Atmos. Environ*., **12**, 549-568.

Jirak, Israel L., and William R. Cotton, 2006: Effect of air pollution on precipitation on precipitation along the Front Range of the Rocky Mountains. *J. Appl. Meteor and Climatology*, **45**, 236-245.

Kaufman, Yoram J., Robert S. Fraser, and Richard A. Ferrare, 1990: Satellite measurements of large-scale air pollution: Methods. *J. Geophys. Res.,* **95**, No. D7, 9895-9909.

King, Michael D., Si-Chee Tsay, Steven E. Platnick, Menghua Wang, and Kuo-Nan Liou, 1997: Cloud retrieval algorithms for MODIS: Optical thickness, effective particle radius, and thermodynamic phase. MODIS Algorithm Theoretical Basis Document No. ATBD-MOD-05, 79 pp.

Kleinman, Lawrence L., and Petere H. Daum, 1991: Oxidant limitation to the formation of H_2SO_4 near a SO_2 source region. *Atmos. Environ.,* **25A**, No. 9, 2023-2028.

Leaitch, W. R., and G. A. Isaac, 1994: On the relationship between sulfate and cloud droplet number concentrations. *J. Clim*., **7**, 206-212.

Leaitch, W. R., G. A. Isaac, J. W. Strapp, C. M. Banic, and H. A. Wiebe, 1992: The relationship between cloud droplet number concentrations and anthropogenic pollution: Observations and climatic implications. *J. Geophys. Res*., **97**, 2463-2474.

Lensky, Itamar M., and Daniel Rosenfeld, 2003: Satellite-based insights into precipitation formation processes in continental and maritime convective clouds at nighttime. *J. Appl. Meteor*., **42**, 1227-1233.

Li, Jun, Hung-Lung Huang, Chian-Yi Liu, Ping Yang, Timothy J. Schmit, Heli Wei, Elisabeth Weisz, Li Guan, and W. Paul Menzel, 2005: Retrieval of Cloud microphysical properties from MODIS and AIRS. *J. Appl. Meteor*., **44**, 1526-1543.

Li, Jun, W. Paul Menzel, Zhongdong Yang, Richard A. Frey, and Steven A. Ackerman, 2003: High-spatial-resolution surface and cloud-type classification from MODIS multispectral band measurements. *J. Appl. Meteor*., **42**, 204-226.

Lohmann, Ulrike, 2004: Can anthropogenic aerosols decrease the snowfall rate? *J. Atmos. Sci*., **61**, 2457-2468.

Lohmann, Ulrike, George Tselioudis, and Chris Tyler, 2000: Why is the cloud albedo – particle size relationship different in optically thick and optically thin clouds? *Geophys. Res. Letters*, **27**, No. 8, 1099-1102.

Lohmann, U., and J. Zhang, 2003: Sensitivity studies of the effect of increased aerosol concentrations and snow crystal shape on the snowfall rate in the Arctic. *J. Geophys. Res*., **108**, No. D11, 4341.

Mamane, Yaacov, and Rudolf F. Pueschel, 1980: Formation of sulfate particles in the plume of the Four Corners Power Plant. *J. Appl. Meteor*., **19**, 779-790.

Mast, M.A., D.H. Campbell, and G.P. Ingersoll, 2005: Effects of emission reductions at the Hayden powerplant on precipitation, snowpack, and surface-water chemistry in the Mount Zirkel Wilderness Area, Colorado, 1995-2003. U.S. Geological Survey Scientific Investigations Report 2005-5167, 32 p.

Mellor, G. L., and T. Yamada, 1974: A hierarchy of turbulence closure methods for planetary boundary layers. *J Atmos Sci*., **31**, 1791-1806.

Mesinger, Fedor, Geoff DiMego, Eugenia Kalnay, Kenneth Mitchell, Perry C. Shafran, Wesley Ebisuzaki, Dusan Jovic, Jack Woollen, Eric Rogers, Ernesto H. Berbery, Michael B. Ek, Yun Fan, Robert Grumbine, Wayne Higgins, Hong Li, Ying Lin, Geoff Manikin, David Parrish, and Wei Shi, 2006: North American Regional Reanalysis. *Bull. Amer. Meteor. Soc*., **87**, No 3., 343-360.

Metzger, S., F. Dentener, M. Krol, A. Jeuken, and J. Lelieveld, 2002: Gas/aerosol partitioning – 2. Global modeling results. *J. Geophys Res*., **107**, No. D16, 4313.

Meyers, M. P., R. L. Walko, J. Y. Harrington, and W. R. Cotton, 1997: New RAMS cloud microphysics parameterization. Part II: The two-moment scheme. *Atmos Res*., **45**, 3-39.

Nakajima, Teruyuki, Akiko Higurashi, Kazuaki Kawamoto, and Joyce E. Penner, 2001: A possible correlation between satellite-derived cloud and aerosol microphysical parameters. *Geophys. Res. Letters*, **28**, No. 7, 1171-1174.

Novakov, T., C. Rivera-Carpio, J. E. Penner, and C. F. Rogers, 1994: The effect of anthropogenic sulfate aerosols on marine cloud droplet concentrations. *Tellus*, **46B**, 132-141.

Pakkanen, Tuomo A., 1996: Study of formation of coarse particle nitrate aerosol. *Atmos. Environ.,* **30**, No. 14, 2475-2482.

Platnick, S., Michael D. King, Steven A. Ackerman, W. Paul Menzel, Bryan A. Baum, Jerome C. Riedi, and Richard A. Frey, 2003: The MODIS cloud products: Algorithms and Examples from Terra. *IEEE Transactions on Geoscience and Remote Sensing*, **41**, No. 2, 459-473.

Platnick, S., J. Y. Li, M. D. King, H. Gerber, and P. V. Hobbs, 2001: A solar reflectance method for retrieving the optical thickness and droplet size of liquid water clouds over snow and ice surfaces. *J. Geophys. Res*., **106**, No. D14, 15,185-15,199.

Pruppacher, H.R., and J.D. Klett, 1978: *Microphysics of Clouds and Precipitation*. D. Reidel Publishing Co., Boston, USA, 714 pp.

Pueschel, R. F., and C. C. Van Valin, 1978: Cloud nucleus formation in a power plant plume. *Atmos. Environ*., **12**, 307-312.

Ramanathan, V., P. J. Crutzen, J. T. Kiehl, and D. Rosenfeld, 2001: Aerosols, climate, and the hydrological cycle. *Science*, **294**, 2119-2124.

Rauber, Robert M., and Lewis O. Grant, 1986: The characteristics and distribution of cloud water over the mountains of northern Colorado during wintertime storms. Part II: Spatial distribution and microphysical characteristics. *J Clim. Appl. Meteor.,* **25**, 489-504.

Rauber, Robert M., Lewis O. Grant, Daxiong Feng, and J. B. Snider, 1986: The characteristics and distribution of cloud water over the mountains of northern Colorado during wintertime storms. Part I: Temporal variations. *J Clim. Appl. Meteor.,* **25**, 468-488.

Rosenfeld, Daniel, 1999: TRMM observed first direct evidence of smoke from forest fires inhibiting rainfall. *Geophys. Res. Letters*, **26**, No. 20, 3105-3108.

Rosenfeld, Daniel, 2000: Suppression of rain and snow by urban and industrial air pollution. *Science*, **287**, 1793-1796.

Rosenfeld, Daniel, and Amir Givati, 2006: Evidence of orographic precipitation suppression by air pollution-induced aerosols in the western United States. *J. Appl. Meteor. and Clim*., **45**, 893-911.

Saleeby, Stephen M., and William R. Cotton, 2005: A large-droplet mode and prognostic number concentration of cloud droplets in the Colorado State University Regional Atmospheric Modeling System (RAMS). Part II: Sensitivity to a Colorado winter snowfall event. *J. Appl. Meteor*., **44**, 1912-1929.

Schatzmann, Michael, and Anthony J. Policastro, 1984: Plume rise from stacks with scrubbers: A state-of-the-art review. *Bull. Amer. Meteor. Soc*., **65**, No. 3, 210-215.

Schnell, R. C., C.C. van Valin, and R. F. Pueschel, 1976: Atmospheric ice nuclei: no detectable effects from a coal-fired power plant plume. *Geophys. Res. Letters*, **3**, 657-660.

Seinfeld, J.H., and S.N. Pandis, *Atmospheric Chemistry and Physics*, Wiley-Interscience, New York, USA, 1998.

Serreze, Mark C., Martyn P. Clark, Richard L. Armstrong, David A. McGinnis and Roger S. Pulwarty, 1999: Characteristics of the western United States snowpack from snowpack telemetry (SNOTEL) data. *Water Resources Res*., **35**, No. 7, 2145-2160.

Smagorinsky, J., 1963: General circulation experiments with the primitive equations. *Mon. Wea. Rev*., **91**, 99-164.

Smith. S. J., H. Pitcher, and T. M. L. Wigley, 2001: Global and regional anthropogenic sulfur dioxide emissions. *Global Planetary Change*, **29**, 99-119.

Stocker, R. A., R. A. Pielke, and M. Uliasz, 1992: Impact of local sources during stagnant conditions in Shenandoah National Park. *Air Pollution Modeling and its Application IX*, H. van Dop and G. Kallos, Eds., Plenum Press, New York, 179-186.

Twomey, S., 1974: Pollution and the Planetary Albedo. *Atmos. Environ.,* **8**, 1251-1256.

Twomey, S. 1977: The influence of pollution on the shortwave albedo of clouds. *J. Atmos. Sci.,* **34**, 1149-1152.

Twomey, S. and J. Warner, 1967: Comparison of measurements of cloud droplets and cloud nuclei. *J Atmos. Sci.,* **24**, 702-703.

Uliasz, Marek, 1993: The atmospheric mesoscale dispersion modeling system. *J. Appl. Meteor*., **32**, 139-149.

Uliasz, M., and R. Pielke, 1990: Receptor-oriented Lagrangian-Eulerian model of mesoscale air pollution. *Computer Techniques in Environmental Studies III*, P. Zanetti, Ed., Computational Mechanics Publications, Southamption, 57-68.

Walko, R. L., L. E. Band, J. Baron, T. G. F. Kittel, R. Lammers, T. J. Lee, D. Ojima, R. A. Pielke Sr., C. Taylor, C. Tague, C. J. Tremback, and P.J. Vidale, 2000: Coupled

atmospheric-biophysics-hydrology models for environmental modeling. *J. Appl. Meteor.*, **34**, 994-999.

Wetzel, M. A., 1995: Simulation of radiances for future AVHRR platforms with the AVIRIS spectral radiometer. *Int. J. Remote Sensing*, **16**, No. 6, 1167-1177.

Wetzel, Melanie, Michael Myers, Randolph Borys, Ray McAnelly, William Cotton, Andrew Rossi, Paul Frisbie, David Nadler, Douglas Lowenthal, Stephen Cohn, and William Brown, 2004: Mesoscale snowfall prediction and verification in mountainous terrain. *Weather and Forecasting*, **19**, 806-827.

Wylie, D. P., and W. P. Menzel, 1999: Eight years of high cloud statistics using HIRS. *J. Climate*, **12**, 170-184.